JOC The Journal of Organic Chemistry

Article

pubs.acs.org/joc

Decoding the Mechanism of Intramolecular Cu-Directed Hydroxylation of sp^3 C−H Bonds

Rachel Trammell,[†,∥] Yi Yang See,[‡,∥] Aaron T. Herrmann,[‡] Nan Xie,[†] Daniel E. Díaz,[§] Maxime. A. Siegler,[§] Phil S. Baran,[‡] and Isaac Garcia-Bosch*[,†]

[†]Department of Chemistry, Southern Methodist University, Dallas, Texas 75275, United States

[‡]Department of Chemistry, The Scripps Research Institute, 10550 North Torrey Pines Road, La Jolla, California 92037, United States

[§]Johns Hopkins University, Baltimore, Maryland 21218, United States

Supporting Information

ABSTRACT: The use of copper in directed C−H oxidation has been relatively underexplored. In a seminal example, Schönecker showed that copper and O_2 promoted the hydroxylation of steroid-containing ligands. Recently, Baran (*J. Am. Chem. Soc.* **2015**, *137*, 13776) improved the reaction conditions to oxidize similar substrates with excellent yields. In both reports, the involvement of Cu_2O_2 intermediates was suggested. In this collaborative article, we studied the hydroxylation mechanism in great detail, resulting in the overhaul of the previously accepted mechanism and the development of improved reaction conditions. Extensive experimental evidence (spectroscopic characterization, kinetic analysis, intermolecular reactivity, and radical trap experiments) is provided to support each of the elementary steps proposed and the hypothesis that a key mononuclear $LCu^{II}(OOR)$ intermediate undergoes homolytic O−O cleavage to generate reactive RO$^\bullet$ species, which are responsible for key C−H hydroxylation within the solvent cage. These key findings allowed the oxidation protocol to be reformulated, leading to improvements of the reaction cost, practicability, and isolated yield.

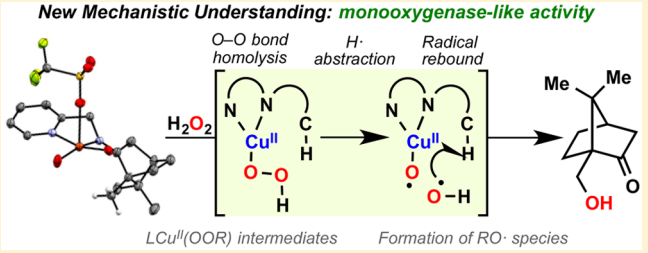

INTRODUCTION

The chemoselective oxidation of C−H bonds is one of the most powerful synthetic tools for the introduction of functionality into complex organic molecules.[1−4] One of the main challenges of this strategy is to develop methods that overcome the intrinsic inertness of certain C−H bonds. Nature has mastered the selective oxygenation of organic molecules using enzymatic machinery with the most prominent examples being iron- and copper-containing metalloenzymes. These proteins couple the oxidation of C−H bonds with the reduction of dioxygen, which serves as both the H^+/e^- acceptor (oxidase activity) and the oxygen-atom source (oxygenase activity) with exquisite chemoselectivity and under physiological conditions.[5,6]

Taking inspiration from these systems, chemists have explored the use of early transition metal complexes as catalysts for the oxidation of C—H and C═C bonds using O_2 or its reduced form (H_2O_2) as the oxidant.[7] While the development of iron catalysts for alkane hydroxylation, alkene epoxidation, and *cis*-dihydroxylation has been achieved with rational ligand design,[8−10] the use of copper systems to catalyze C—H and C═C oxidations has been less explored.[11−14] Recently, we reported that Cu^I complexes bearing pyridinic tetradentate ligands could catalyze the oxidation of alkanes with strong C—H bonds (i.e., cyclohexane) using H_2O_2 as the oxidant.[15] Mechanistic studies pointed toward a Fenton-like peroxidative mechanism, which excluded the use of this catalytic system in the oxidation of complex substrates with multiple C—H bonds because of the nonselective nature of the hydroxyl radical (HO$^\bullet$).

One of the milestone reports in practical copper-mediated C−H oxidation is by Schönecker and co-workers (Figure 1).[16−18] Derivatization of the C17 ketone of steroid substrates to generate a bidentate imino-pyridine ligand combined with the addition of a Cu^I source (or Cu^{II} + reductant) and dioxygen led to the selective hydroxylation of C12 with modest yields (up to 50%). This has subsequently been exploited in several impressive syntheses.[19−21] As part of a natural product synthesis effort, the Baran group reinvestigated this interesting oxidation after a vast exploration of alternative methods and strategies failed. The reaction conditions were subsequently improved (ascorbic acid as reductant, shorter reaction times, and higher yields) and applied to the first synthesis of highly oxygenated polyoxypregnane steroids with useful biological properties.[22] In these disclosures, it was proposed that the oxidation proceeded via formation of Cu_2O_2 species, which are considered 2e$^-$ oxidants, limiting the reaction yields to 50% (in Baran's approach, the reductant provided the electrons necessary to overcome the 50% threshold). However, the

Received: May 3, 2017
Published: June 27, 2017

DOI: 10.1021/acs.joc.7b01069
J. Org. Chem. 2017, 82, 7887−7904

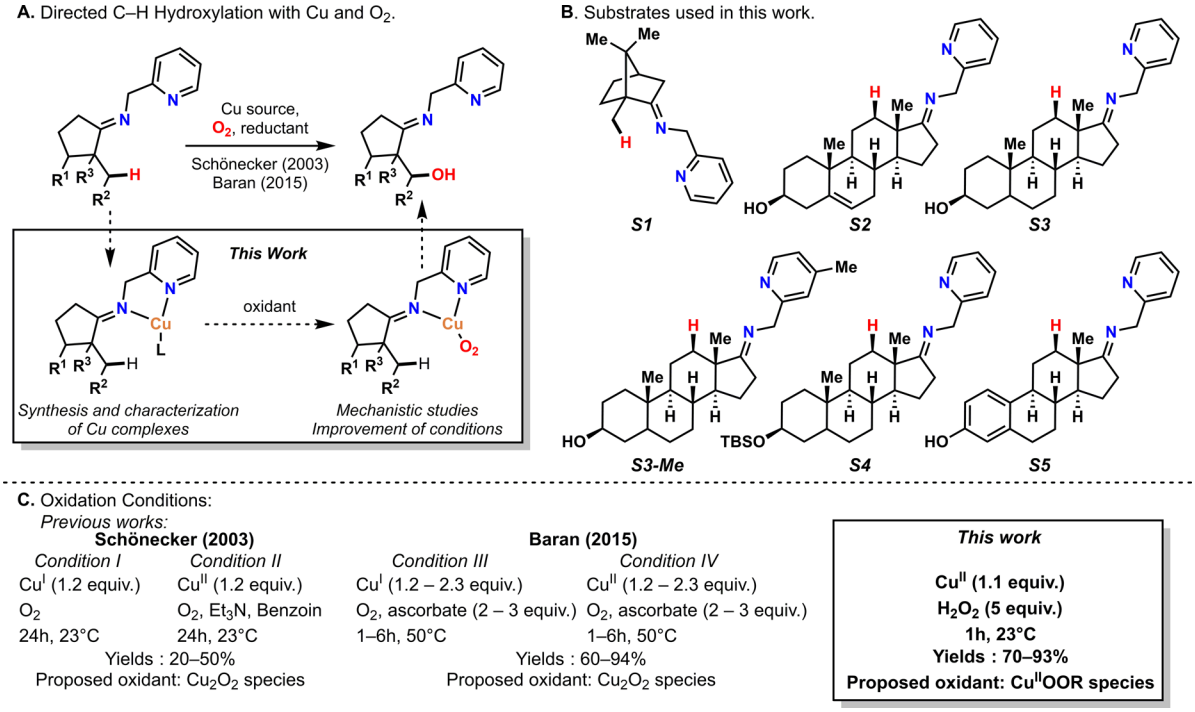

Figure 1. (A) Directed hydroxylation of C−H bonds mediated by Cu and the approach used in this work.[16,22] (B) Substrate-containing ligands used in this work. (C) Oxidative conditions developed by Schönecker[16] (left) and Baran[22] (middle) and improvements described in this work.

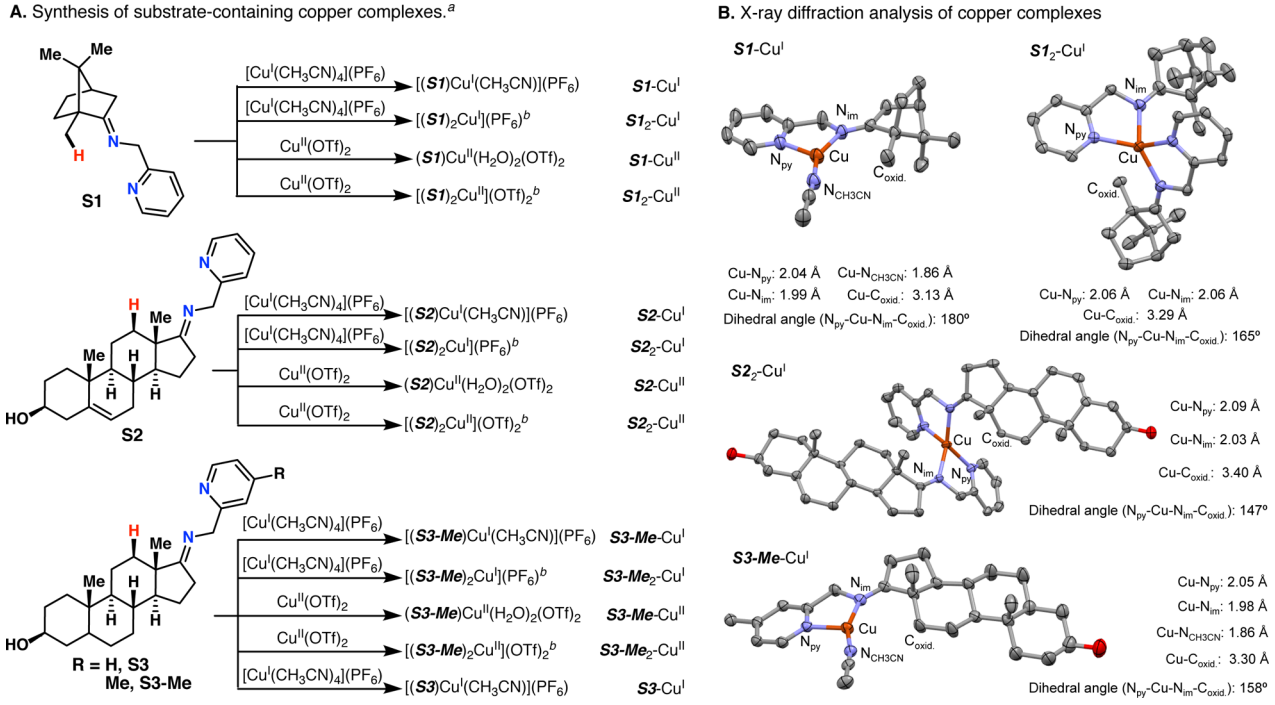

Figure 2. (A) Synthesis of substrate-containing copper complexes. (B) X-ray diffraction analysis of the Cu complexes (displacement ellipsoid plots, 50% probability). For clarity, some anions, disorder, lattice solvent molecules, and H atoms are not depicted. [a]Reaction conditions: 1.0 equiv of Cu salt was used unless otherwise stated (acetone/Et_2O); [b]0.5 equiv of Cu salt was used. See the SI for further details.

general uncertainty surrounding the mechanism has prevented further development of this potentially useful methodology, and advances have been limited to the above-mentioned examples.

In this article, we report our investigation of the mechanism by which Cu, in combination with O_2, oxidizes the C−H bond in these imino-pyridine systems. Various copper complexes bearing different substrate ligands were prepared independently (Figure 1) and used in combination with various oxidative conditions. The substantial data obtained pointed toward a mechanism that is different from the previous proposal that suggested the involvement of Cu_2O_2 species. Spectroscopic characterization of the reaction intermediates, reaction kinetic analysis, and other experimental observations allowed us to

DOI: 10.1021/acs.joc.7b01069
J. Org. Chem. 2017, 82, 7887−7904

A. Oxidation of ***S1*** using previously reported conditions.

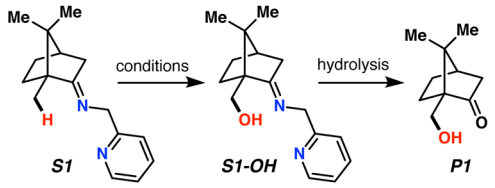

Oxidation Conditions:

Schönecker (2003)		Baran (2015)	
Condition I	*Condition II*	*Condition III*	*Condition IV*
[***S1***] = 137 mM	[***S1***] = 46 mM	[***S1***] = 150 mM	[***S1***] = 150 mM
Cu^{I} (1.2 equiv)	Cu^{II} (1.2 equiv)	Cu^{I} (2.3 equiv)	Cu^{II} (2.3 equiv)
O_2, 24h, 23°C	O_2, 24h, 23°C, Et_3N, benzoin (2 equiv)	O_2, 6h, 50°C, NaAsc (3.0 equiv)	O_2, 6h, 50°C, NaAsc (3.0 equiv)
31%	**4%**	**94%**	**87%**

B. Oxidation of Cu/***S1*** complexes.

Entry	*Cu/S1 complex*	*Conditions*[a]
1	***S1***-Cu^{I}	O_2, 0 °C, 6h
2	***S1***-Cu^{I}	O_2, 20 °C, 6h
3	***S1***-Cu^{I}	O_2, 50 °C, 6h
4	***S1***-Cu^{I}	O_2, 50 °C, 6h, CH_3CN
5	***S1***-Cu^{I}	O_2, 50 °C, 6h, CH_2Cl_2
6	***S1***-Cu^{I}	O_2, 50 °C, 6h, MeOH/Acetone (1:1)
7	***S1***-Cu^{I}	O_2, 50 °C, 6h; Cu^{I} (1 equiv)
8	***S1***-Cu^{I}	O_2, 50 °C, 6h, NaAsc (1 equiv)
9	***S1***-Cu^{I}	H_2O_2 (1.2 equiv), 20 °C, 0.5h
10	***S1***-Cu^{I}	H_2O_2 (2.5 equiv), 20 °C, 0.5h
11	***S1***-Cu^{I}	H_2O_2 (3.75 equiv), 20 °C, 0.5h
12	***S1***-Cu^{I}	H_2O_2 (5.0 equiv), 20 °C, 0.5h
13	$S1_2$-Cu^{I}	O_2, 20 °C, 6h
14	$S1_2$-Cu^{I}	O_2, 50 °C, 6h
15	$S1_2$-Cu^{I}	O_2, 20 °C, 6h, Cu^{I} (1 equiv)
16	$S1_2$-Cu^{I}	H_2O_2 (5.0 equiv), 20 °C, 0.5h
17	***S1***-Cu^{II}	O_2, 50 °C, 6h
18	***S1***-Cu^{II}	H_2O_2 (5.0 equiv), 20 °C, 0.5h
19	$S1_2$-Cu^{II}	O_2, 50 °C, 6h
20	$S1_2$-Cu^{II}	H_2O_2 (5.0 equiv), 20 °C, 0.5h

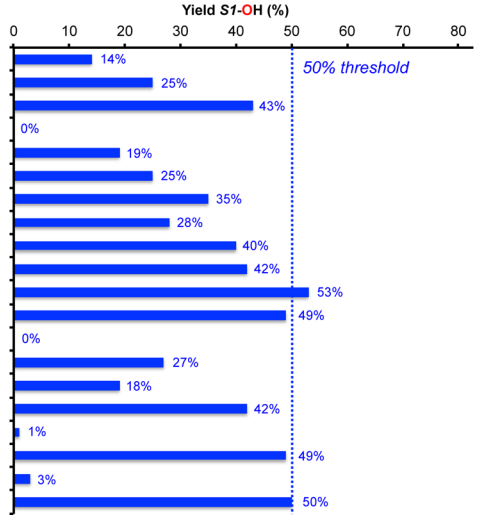

Figure 3. (A) Oxidation of the **S1** substrate described in previous reports.[17,22] (B) Results obtained in the oxidation of the different **S1**-derived copper complexes (hydroxylation product **S1**−OH in blue) under different conditions. [a]the following reaction conditions were used unless otherwise stated: [**S1**] = 4.0 mM in anhydrous acetone. See the SI for further details.

propose a new mechanistic framework in which the intramolecular substrate oxidation was promoted in a mononuclear fashion, similar to that proposed for the oxidation of C−H bonds in some Cu-dependent monooxygenase enzymes such as peptidylglycine-α-hydroxylating monooxygenase (PHM) or lytic polysaccharide monooxygenase (LPMO).[23] With this new understanding, the oxidation conditions were reoptimized, leading to improvements in practicability, cost, and product yields. Most importantly, the studies described herein are the most complete picture to date of this fascinating but largely mysterious C−H oxidation.

RESULTS AND DISCUSSION

Synthesis of Substrate-Containing Cu Complexes. A series of camphor-imine-pyridine-derived (**S1**-derived) copper complexes was synthesized by mixing 1 or 2 equiv of bidentate ligand **S1** with Cu sources $[Cu^{I}(CH_3CN)_4](PF_6)$ or $Cu^{II}(CF_3SO_3)_2$ in acetone (Figure 2A). X-ray-quality crystals of the **S1**-derived Cu complexes could be obtained by layering diethyl ether on acetone solutions of the compounds (see Figure 2). Complex **S1**−Cu^{I} was found to have the copper ion in a distorted T-shaped geometry, with a short Cu−$NCCH_3$ distance (1.86 Å). The Cu ion, the three N donors, and the C atom that undergoes the C−H oxidation (C_{oxid}) were found in the same plane (dihedral angle: 180°), with the latter C atom close to the Cu ion (Cu−C_{oxid}: 3.13 Å).

The **S1**-derived copper complexes were fully characterized by different spectroscopic and spectrometric means, including ^{1}H NMR (for Cu^{I} complexes), UV−vis, ESI-MS, and elemental analysis (see the Supporting Information for details). For the L/Cu^{I} and L_2/Cu^{I} complexes, distinctive ^{1}H NMR spectra were found for each of the species, with the peaks shifting downfield for the **S1**−Cu^{I} complex. The UV−vis spectra of the **S1**-derived Cu complexes were also very distinctive depending on the oxidation state and number of **S1** ligands coordinated to the metal center. This resulted in the complexes having distinctive colors with the $[(\mathbf{S1})Cu^{I}(CH_3CN)](PF_6)$ (**S1**−Cu^{I}) as pale yellow, $[(\mathbf{S1})_2Cu^{I}](PF_6)$ ($\mathbf{S1}_2$−Cu^{I}) as intense yellow, $[(\mathbf{S1})Cu^{II}(H_2O)_2(CF_3SO_3)](CF_3SO_3)$ (**S1**−Cu^{II}) as blue, and $[(\mathbf{S1})_2Cu^{II}](CF_3SO_3)$ ($\mathbf{S1}_2$−Cu^{II}) as green (see the SI for further details). The distinctive spectroscopic features of these complexes enabled us to use these signatures during the oxidation reactions to identify the Cu oxidation state as well as ligand coordination number.

The synthesis of the steroid-imino-pyridine Cu complexes was carried out similarly to those of the **S1**-derived analogues (**S2**, **S3**, and **S3**−Me; Figure 2A; see the SI for further details). The **S2**/**S3**−Me Cu complexes also had distinctive colors depending on the oxidation state (Cu^{I}/Cu^{II}) and the number of ligands coordinated to the Cu ion (see the SI). X-ray diffraction analysis (Figure 2B) of **S3**−Me−Cu^{I} found a Cu^{I} ion coordinated in a T-shaped fashion, with 3 nitrogen donors (2 from the bidentate ligand, and CH_3CN) and the metal center occupying the same plane. Like in **S1**−Cu^{I}, the C atom that is oxidized (C_{oxid}; C12 steroid numbering) is close to the Cu^{I} ion (3.30 Å) although it was found slightly above the plane formed by the Cu and N donors (dihedral angle: 158°). The steroid-imino-pyridine complexes (Figure 2B) were also fully characterized by various spectrometric and spectroscopic means.

It is also worth mentioning that the isolation of copper complexes bearing similar ligands has been challenging.[24,25] To the best of our knowledge, this work constitutes a unique example of a detailed structural and spectroscopic character-

DOI: 10.1021/acs.joc.7b01069
J. Org. Chem. 2017, 82, 7887−7904

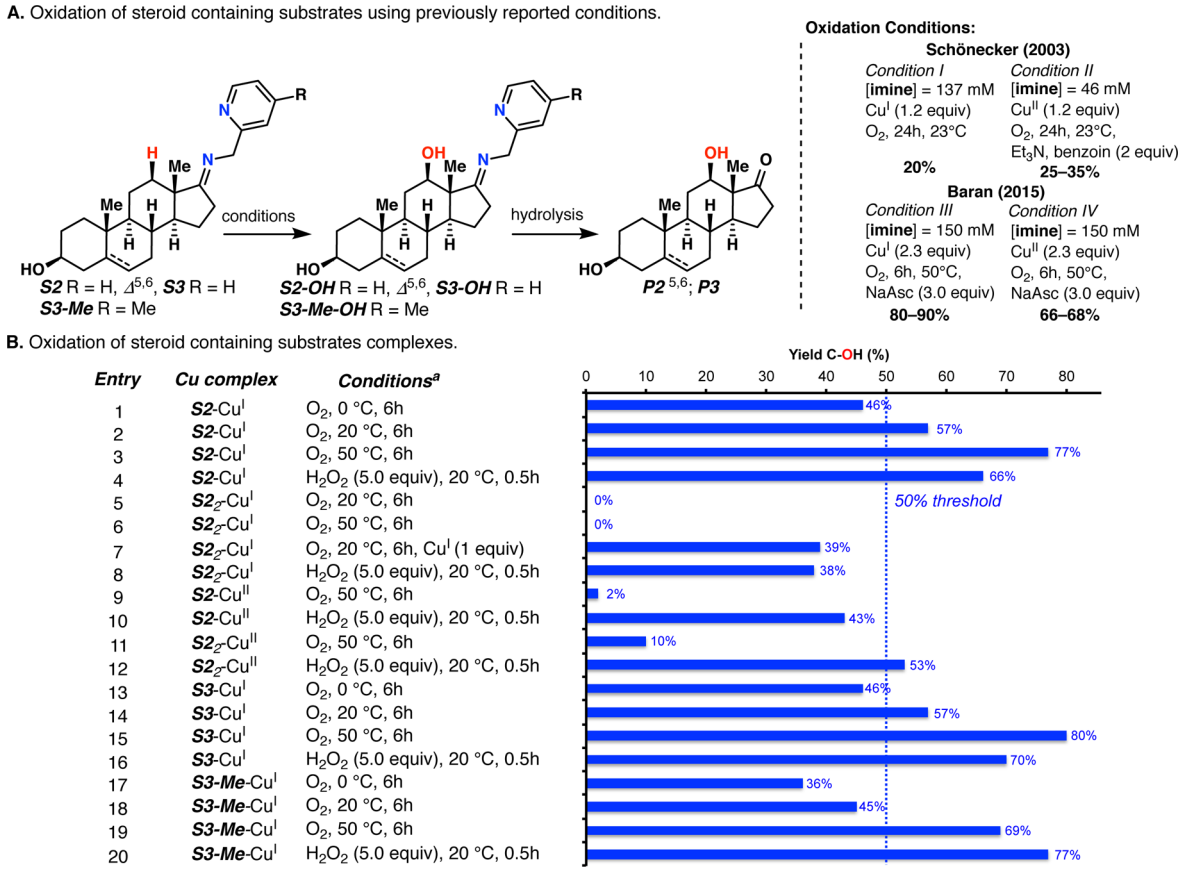

Entry	Cu complex	Conditions[a]
1	**S2**-Cu^{I}	O_2, 0 °C, 6h
2	**S2**-Cu^{I}	O_2, 20 °C, 6h
3	**S2**-Cu^{I}	O_2, 50 °C, 6h
4	**S2**-Cu^{I}	H_2O_2 (5.0 equiv), 20 °C, 0.5h
5	**S2**$_2$-Cu^{I}	O_2, 20 °C, 6h
6	**S2**$_2$-Cu^{I}	O_2, 50 °C, 6h
7	**S2**$_2$-Cu^{I}	O_2, 20 °C, 6h, Cu^{I} (1 equiv)
8	**S2**$_2$-Cu^{I}	H_2O_2 (5.0 equiv), 20 °C, 0.5h
9	**S2**-Cu^{II}	O_2, 50 °C, 6h
10	**S2**-Cu^{II}	H_2O_2 (5.0 equiv), 20 °C, 0.5h
11	**S2**$_2$-Cu^{II}	O_2, 50 °C, 6h
12	**S2**$_2$-Cu^{II}	H_2O_2 (5.0 equiv), 20 °C, 0.5h
13	**S3**-Cu^{I}	O_2, 0 °C, 6h
14	**S3**-Cu^{I}	O_2, 20 °C, 6h
15	**S3**-Cu^{I}	O_2, 50 °C, 6h
16	**S3**-Cu^{I}	H_2O_2 (5.0 equiv), 20 °C, 0.5h
17	**S3-Me**-Cu^{I}	O_2, 0 °C, 6h
18	**S3-Me**-Cu^{I}	O_2, 20 °C, 6h
19	**S3-Me**-Cu^{I}	O_2, 50 °C, 6h
20	**S3-Me**-Cu^{I}	H_2O_2 (5.0 equiv), 20 °C, 0.5h

Figure 4. (A) Oxidation of the steroid-containing substrates described in previous reports.[17,22] (B) Results obtained in the oxidation of the different steroid-derived copper complexes (hydroxylation product C−OH in blue) under different conditions. [a]the following reaction conditions were used unless otherwise stated: [Cu complex] = 4.0 mM in dry acetone. See the SI for further details.

ization of copper(I) and copper(II) complexes bearing imino-pyridine scaffolds.

Oxidations under Different Reaction Conditions. *Oxidation of* ***S1****-Derived Complexes.* In their seminal report, Schönecker and co-workers reported that **S1** was a more challenging substrate than the steroid-derived analogues.[17] Using their reaction conditions (Figure 3A), **S1** was oxidized with modest yields (4−31%). Baran and co-workers were able to reach higher oxidation yields (up to 94%) by varying the reaction conditions developed for the oxidation of steroid-containing systems (i.e., higher Cu and reductant loadings and longer reactions times).[22]

Deoxygenated solutions of the Cu complexes (4 mM) were exposed to the chosen oxidant (e.g., bubbling O_2), with stirring for a predetermined period of time (i.e., 30 min to 6 h). The resulting reaction mixture was then decomplexed using Baran's procedure (aqueous Na_4EDTA solution)[22] and analyzed by ^1H NMR (Figure 3).

A substantial increase in the yield of **S1**−OH was observed with increasing temperature (14% at 0 °C, 25% at 20 °C, and 43% at 50 °C; entries 1−3, Figure 3). In all these cases (0, 20, and 50 °C), immediate oxidation to Cu^{II} was observed (green color, *vide supra*) upon addition of O_2 to the Cu^{I} complex. This was the first piece of evidence against the previous mechanistic proposals: Cu_2O_2 species are typically formed and observed at low temperatures (−40 to −130 °C) and usually decay rapidly at room temperature to form Cu^{II} products. Therefore, no yield difference should be observed between 0 and 50 °C after long reaction times.[26,27]

Then, the effect of different solvents on the reaction yields was evaluated (entries 2−6, Figure 3). While no difference was observed when MeOH was used as cosolvent with acetone (entry 2, 25%, versus entry 6, 25%), a slight decrease was observed when the reaction was carried out in CH_2Cl_2 (entry 5, 19%). No oxidation products were detected in the oxidation of **S1**−Cu^{I} in CH_3CN (entry 4). Furthermore, no color change was observed over the course of 6 h with O_2 bubbling, indicating no reaction with O_2. Consequently, we speculate that the dissociation of CH_3CN in **S1**−Cu^{I} is crucial prior to the O_2 binding and subsequent oxidation.

Lastly, we evaluated the impact of external reductants on the reaction. In the presence of 1 equiv of Cu^{I} source (entry 7), or 1 equiv of ascorbate (entry 8), a slight increase in the product yields was observed (3−10% increase).

Next, we hypothesized that the temperature dependence of the reaction yields could be due to the formation of hydroperoxide species derived from solvent oxidation during the reaction: the formation of peroxides in the presence of metal complexes and O_2 is well-documented in solvents such as acetone, and is usually increased at higher temperatures.[28] In fact, when H_2O_2 was used as the oxidant instead of O_2, a substantial increase in yields was observed (entries 9−12, Figure 3). When the H_2O_2 concentration was increased to 15 mM, the observed yield surpassed the 50% threshold (entry 11, 53%). Further increases in the H_2O_2 concentrations led to the quantitative consumption of **S1**, but overoxidation of the **S1**−OH product was also observed, leading to a net decreased final yield (entry 12, 47%; see the SI for details). Interestingly, these

DOI: 10.1021/acs.joc.7b01069
J. Org. Chem. 2017, 82, 7887−7904

modifications led to higher yields at room temperature than that obtained at 50 °C with O_2, with the concomitant and substantial reduction in the reaction times (6 h versus 30 min).

The oxidation of the other **S1**-derived complexes was also examined. **S1**$_2$−Cu^I did not react with O_2 to generate the **S1**−OH product at room temperature. In fact, no color change was observed (see the SI for UV−vis analysis). However, when the same procedure was repeated at 50 °C, the solution turned green, and the hydroxylated product of **S1** was observed (27% yield). This is highly suggestive of an equilibrium between the L_2/Cu^I and the L/Cu^I complexes, with the latter being susceptible to oxidation by O_2. For support of this hypothesis, the oxidation of **S1**$_2$−Cu^I with O_2 in the presence of 1 equiv of Cu^I was performed. Accordingly, the formation of the hydroxylation product at room temperature was observed (entry 15, 18% yield), indicating that the presence of Cu^I shifted the equilibrium toward the oxidatively active L/Cu^I complex ($L_2Cu^I + Cu^I = 2LCu^I$). The oxidation of the **S1**$_2$−Cu^I complex with H_2O_2 (entry 16, Figure 3) was also examined: an excess of oxidant (5 equiv; [H_2O_2], 20 mM) led to a remarkable oxidation yield (42%). Again, we propose that the equilibrium between the L_2/Cu and L/Cu complexes was pushed toward the formation of the L/Cu^I complex, which reacted with H_2O_2 to oxidize the ligand scaffold.

Finally, the oxidation of the cupric complexes was studied using O_2 and H_2O_2 (entries 17−20, Figure 3). Both **S1**−Cu^{II} and **S1**$_2$−Cu^{II} were found to be unreactive with O_2 at room temperature, and only led to very low yields even at 50 °C (yields < 5%). On the other hand, the addition of 5 equiv of H_2O_2 led to good yields (up to 50%). This result is in agreement with Cu^I serving as an electron source to generate H_2O_2 in solution, which is responsible for the oxidation of the ligand through Cu^{II} to the hydroxylation products. These findings were also crucial to the redesign of a new experimental protocol based on Cu^{II} salts and hydrogen peroxide (*vide infra*).

Oxidation of Steroid-Derived Complexes. Similar to that of the **S1** analogues, the oxidation of the steroid-derived Cu complexes under different reaction conditions was examined (Figure 4). Schönecker and co-workers reported very modest yields (20−35%) despite the long reaction times (24 h).[16,17] Baran and co-workers substantially improved the yields (70−90%) and shortened the reaction times (1.5 h at 50 °C) by increasing temperature, the amount of copper (1.3 equiv), and reductant loadings (2.0 equiv).[22]

As with that of **S1**, the oxidation of **S2**−Cu^I with O_2 at different temperatures was studied (entries 1−3, Figure 4). Even at low temperatures, the reaction yields were substantially higher than that for the **S1** substrate (0 °C, 46%), indicative of the higher reactivity of the steroidal systems. Strikingly, the reaction yields were very high (60−80%) at higher reaction temperatures (20−50 °C). Because the obtained oxidation yields were temperature-dependent and the product quantity reached percentages far beyond the 50% threshold, this data was a strong indication that the previous mechanistic proposal, which invoked the formation of Cu_2O_2 species, was improbable (i.e., according to the previous proposals, only 50% C−OH yield could be reached under stoichiometric amounts of the Cu source). Similar C−OH yields beyond the 50% threshold were obtained when the oxidation of **S2**−Cu^I was carried out with H_2O_2 as the oxidant (entry 4, 66%). The remaining **S2**-derived copper complexes were also exposed to the oxidative conditions, and the C−OH reaction yields are summarized in Figure 4 (entries 5−12).

Similar to before, the inertness of **S2**$_2$−Cu^I to O_2 (0% yield at 50 °C) could be circumvented by adding 1 equiv of Cu^I (entry 7, 39%) or using H_2O_2 as the oxidant (entry 8, 38%). The **S2**−Cu^{II} complex was not oxidized by O_2 at high temperatures (entry 9, yield < 5%), but the usage of H_2O_2 (20 mM, 30 min) led to the formation of the oxidation product (entry 10, 43%). Finally, the oxidation of **S2**$_2$−Cu^{II} could not be accomplished when O_2 was used as the oxidant (entry 11, yield < 5%), but reaction with H_2O_2 led to the hydroxylation of the C12 position (entry 12, yield = 53%). The reactivities of the **S3**-derived and **S3**−Me-derived Cu^I complexes were found to be similar to the **S2**−Cu^I complex with the oxidation yields of **S3**−Cu^I with O_2 showing a dependence on the temperature, varying from 46% (0 °C) to 80% (50 °C) (entries 13−20, Figure 4). The oxidation of **S3**−Me−Cu^I with O_2 followed a similar trend when varying the temperature from 0 to 20 and 50 °C (36%, 45%, and 69% yield, respectively). **S3**−Cu^I and **S3**−Me−Cu^I were also oxidized when exposed to H_2O_2 (20 mM, 30 min), reaching yields beyond the 50% threshold (entries 16 and 20, 70−80%).

Proposed Reaction Mechanism. In previous experimental and computational studies, it was suggested that the Cu-directed C−H oxidation of the imino-pyridine substrates was carried out by dinuclear Cu_2O_2 species (Figure 5A).[17,22,29] The

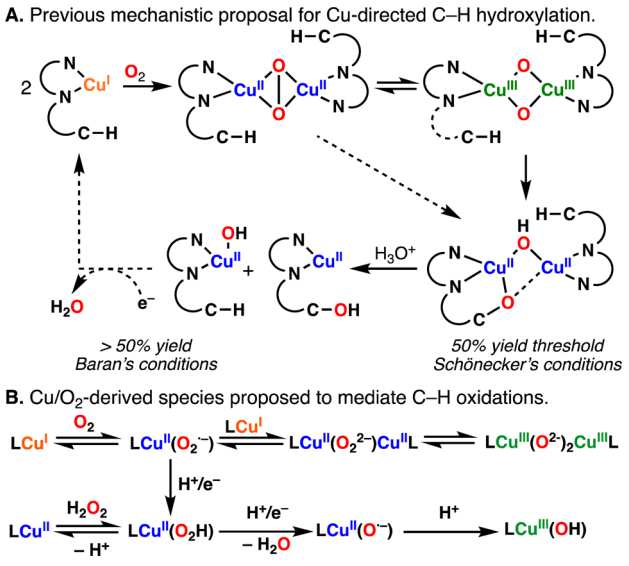

Figure 5. (A) Previous mechanistic proposal[17,22] (Cu_2O_2 intermediacy) for the oxidation of the substrate-containing ligands used in this work. (B) Cu/O_2-derived species proposed to carry out the hydroxylation of C−H bonds in natural systems[5] and model complexes.[32]

proposed mechanistic scenario was mainly based on the stoichiometry of the reaction (yields < 50%) and on the tendency of LCu^I complexes bearing bidentate ligands (e.g., **S1**−**S5**) to form $L_2Cu_2O_2$ species [i.e., $L_2Cu^{II}_2(O_2^{2-})$ and $L_2Cu^{III}_2(O^{2-})_2$].[26,27,30,31] However, no detailed mechanistic study (e.g., characterization of LCu/O_2-derived species) was performed to validate the reaction pathways that led to C−H oxidation.

In addition to $L_2Cu_2O_2$ species, we questioned if mononuclear LCu/O_2-derived species could be involved in the intramolecular hydroxylation of the copper-substrate-imino-pyridine complexes. There has been an increased interest to elucidate the structure and reactivity of mononuclear copper−

DOI: 10.1021/acs.joc.7b01069
J. Org. Chem. 2017, 82, 7887−7904

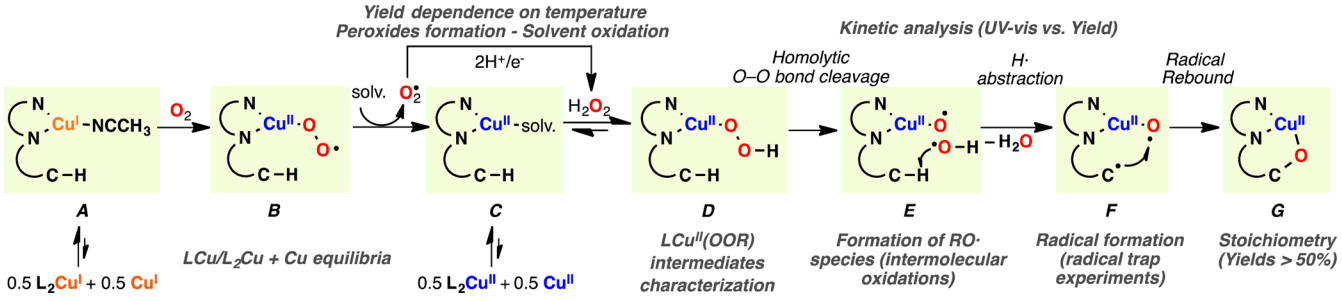

Figure 6. Mechanistic scenario proposed in this work [mononuclear $LCu^{II}(OOH)$ intermediacy] on the basis of the new mechanistic evidence (in gray).

O_2 species,[5,23,33,34] and several research groups have shown that mononuclear LCu/O_2 intermediates, including $LCu^{II}(O_2^{\bullet-})$,[35−37] $LCu^{II}(OOH)$,[38,39] $LCu^{II}(O^{\bullet})$,[40−42] and $LCu^{III}(OH)$,[43] can carry out the intra- and intermolecular oxidations of C−H bonds (Figure 5B).

Taken together, the consistent reactivity trends in the oxidation of the camphor- and steroid-derived Cu complexes (**S1**−**S3**/Cu) described above strongly suggest that an alternative pathway is warranted (Figure 6). In the following sections, we will provide evidence for the mechanism depicted in Figure 6, which is based on the following three concepts.

i. Cu/Ligand Equilibria. The oxidation results described above (Figures 3 and 4) support the idea of an equilibrium between the LCu and the L_2Cu species, in which LCu species are favored. Of the major L_xCu_x species, only the LCu^{I} systems are reactive with O_2 to generate the hydroxylation products. The results obtained in the titration experiments (see the SI) confirm the hypothesis that, in solution, the main species (>80%) are the monoligated LCu complexes when equimolar amounts of Cu and the substrates are mixed. These findings have implications in the design of oxidative conditions: with the present protocol, these substrates cannot be oxidized under catalytic amounts of Cu, and in some cases, additional equivalents of Cu were required to reach high oxidation yields (i.e., Baran reported that 2.3 equiv was required to oxidize **S1**).[22]

ii. LCu^{I}/O_2 Reactions. The observed yields (>50%) and the temperature dependence on the product formation in the oxidation of the LCu^{I} complexes with O_2 were the first indication that the implication of Cu_2O_2 species in the hydroxylation of C−H was questionable. Herein, we proposed that the reaction of LCu^{I} with O_2 leads initially to the formation of a transient Cu^{II}-superoxide intermediate (Figure 6, species **B**) that is converted to the corresponding LCu^{II} complex by releasing free superoxide, which will be converted to H_2O_2 by oxidizing the solvent. Critically, we argue that it is the reaction between the LCu^{II} complex and H_2O_2 that leads to the intramolecular oxidation event.[33]

iii. $LCu^{II}(OOH)$ Formation and Reactivity. The intermediacy of copper(II)-hydroperoxide intermediates (species **D**, Figure 6) is supported by the experimental data from spectroscopic characterization and kinetic analysis of the reaction spectral changes with a correlation to the reaction yields (*vide infra*). Moreover, a series of $LCu^{II}(OOR)$ complexes generated using different ROOH oxidants (in combination with isolated LCu^{I} and LCu^{II} complexes) displayed spectroscopic and reactivity features identical to those of the intermediates formed in the oxidation of LCu^{I} with O_2. Experimental evidence suggests that the different $LCu^{II}(OOR)$ species experience homolytic O−O bond cleavage that generates different oxygen-centered radicals ($RO^{\bullet}$), which are involved in hydrogen-atom abstraction (intermediate **E**, Figure 6). Finally, the carbon-centered radical generated (species **F**, Figure 6) rebounds in an intramolecular fashion with the LCu^{II}-oxyl moiety to form the C−O bond (species **G**, Figure 6).

H_2O_2 Formation (Oxidation of Solvent). Detailed NMR and GC analyses of the crude reactions obtained in the oxidation of **S1**−Cu^{I} and **S2**−Cu^{I} with O_2 led to the detection and quantification of the organic products derived from acetone oxidation (Figure 7).[44] A clear correlation between the substrate oxidation yields and the quantified amounts of acetic acid and hydroxyacetone were also found. At 0 °C, small amounts of acetone oxidation products were detected, suggesting that H_2O_2 is generated by superoxide disproportionation (only $HO_2^{\bullet} = 0.5H_2O_2 + O_2$). At 50 °C, substantial amounts of acetone oxidation were found (up to 70% per Cu

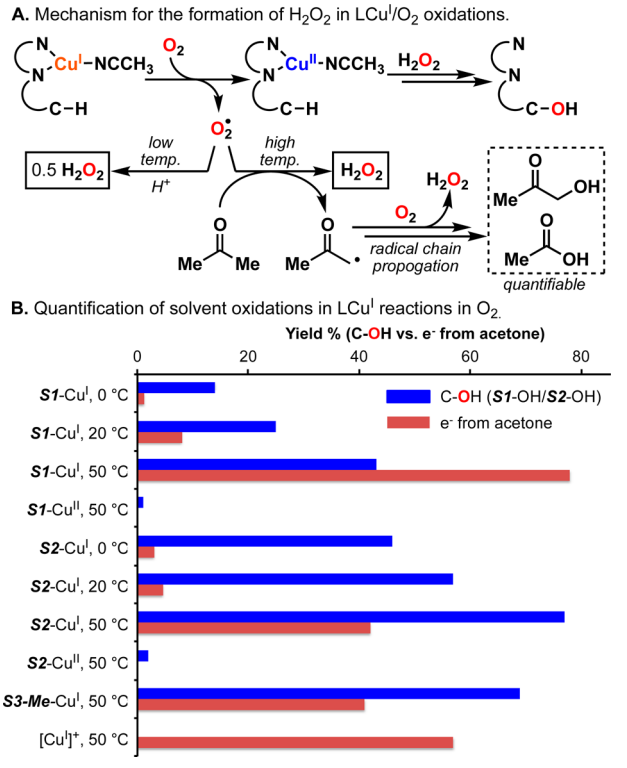

Figure 7. (A) Mechanism of H_2O_2 formation derived from the reaction of the Cu^{I} complexes with O_2. (B) Quantification of the electrons provided by acetone (oxidation of acetone to hydroxyacetone and acetic acid). See the SI for details.

DOI: 10.1021/acs.joc.7b01069
J. Org. Chem. 2017, 82, 7887−7904

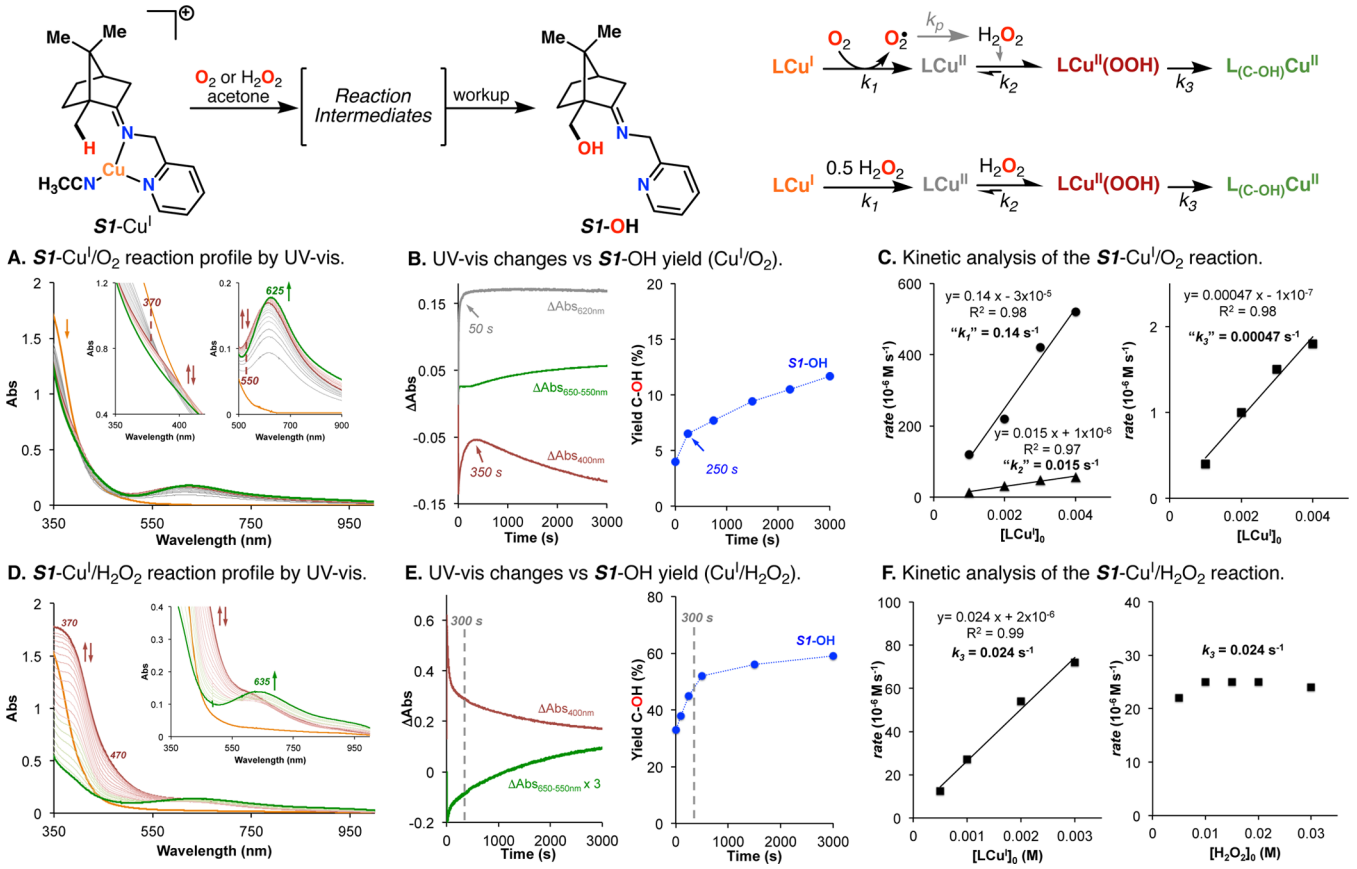

Figure 8. Oxidation of **S1**−Cu^I with O_2 or H_2O_2 at 0 °C. **S1**−Cu^I/O_2: (A) UV−vis spectral changes; (B) variation of the absorbance at selected wavelengths (left) and evolution of the reaction yield (**S1**−OH); (C) kinetic analysis. **S1**−Cu^I/H_2O_2: (D) UV−vis spectral changes; (E) variation of the absorbance at selected wavelengths (left) and evolution of the reaction yield (**S1**−OH); (F) kinetic analysis. It is noted that the evolution of the reaction yield was carried out at 0 °C ($[\mathbf{S1}-Cu^I]_0$ = 4 mM); the first quantification was done at t = 10 s. See text and the SI for details.

center). This is consistent with the endergonic nature of the hydrogen-atom abstraction from acetone (bond-dissociation energy, BDE_{C-H} = 94 kcal/mol)[45] to superoxide to give hydrogen peroxide ($BDE_{(HOO-H)}$ = 91 kcal/mol),[46] which would be favored at higher temperatures. Consequently, the electrons provided by the solvent ($2e^-$ for hydroxyacetone and $4e^-$ for acetic acid) led to higher H_2O_2 formation, and the hydroxylation yields surpass the 50% threshold (see the SI for the putative mechanism by which acetone provides electrons and protons).

Spectrochemical titration methods were used to evaluate the formation of H_2O_2 in the oxygenation of the different substrate-containing copper complexes (see the SI for details). However, we were not able to quantify any substantial amounts. This is consistent with the kinetic data reported below that suggests that slow H_2O_2 formation and rapid H_2O_2 trapping by LCu^{II} preclude its accumulation in solution. Of note, there is a strong solvent effect in the yields obtained during the oxidation of the **S1**−Cu^I and **S2**−Cu^I complexes (see Scheme S16 and Table S16 in the SI for further details). Solvents prone to generate peroxides in solution (e.g., THF, acetone) led to higher hydroxylation yields (40−80%).[28] In the oxidations carried out with benzene and toluene, very poor hydroxylation yields were observed (<10%) despite the observation of the oxidation of LCu^I complexes after being exposed to O_2 (colorless Cu^I solutions turned green). This supports our mechanistic proposal, as O-centered radicals (i.e., superoxide) could be quenched by aromatic solvents to form oxidation products and thus would not give the active oxidant H_2O_2 (see the SI for further details).[15,47,48]

Kinetic Analysis of the Oxidation of the Copper Complexes: Formation of Putative LCu^{II}(OOR) Species Followed by UV−Vis and Evolution of Reaction Yields over Time. Further mechanistic insights into the hydroxylation mechanism were obtained by following the UV−vis spectral changes during the reaction of different **S1**−Cu^I and **S2**−Cu^I complexes under different conditions (i.e., O_2 or H_2O_2 as the oxidants). In a parallel experiment, the evolution of the hydroxylation product over time was also tracked in order to establish at which point the C−H oxidation occurs. In order to capture traces of any fleeting Cu/O_2 species,[26,27] a series of oxygenation experiments at different temperatures (from −135 °C to room temperature), using different solvents (acetone, THF, CH_2Cl_2, and Me−THF) under various reaction conditions (i.e., generation of the Cu^I complexes *in situ*, various Cu^I sources; see the SI for details), were examined.[49] Under no conditions did we observe the formation of any Cu_2O_2 species. This suggested that Cu_2O_2 species are not involved in the intramolecular oxidation of our substrates, but their formation cannot be fully ruled out.

*Oxidation of **S1**−Cu^I with O_2.* First, the reaction of **S1**−Cu^I with O_2 at 0 °C (Figure 8) was monitored by UV−vis. Bubbling O_2 through a precooled solution of the Cu^I complex in acetone (1 mM) led to the spectral changes depicted in Figure 8A. During the first 50 s, the spectral features corresponding to the initial Cu^I species (orange spectrum)

DOI: 10.1021/acs.joc.7b01069
J. Org. Chem. 2017, 82, 7887−7904

rapidly disappeared with the concomitant formation of a species with UV−vis features centered at 610 nm (gray spectra, Figure 8). This first oxidation process was followed by the formation and accumulation (300 s) of a new species (brown spectrum, Figure 8) with a broad UV−vis band at high energies 350−400 nm, and a shoulder at 550 nm (second intermediate). After 300 s, this intermediate slowly decayed, with the concomitant formation of a Cu species with a low energy band at 625 nm (green spectrum, Figure 8). All the collected spectra suggested that the oxidation of **S1**−Cu^{I} with O_2 occurred in a multistep fashion with the involvement of at least two intermediate species.

In a parallel experiment, we quantified the hydroxylation product **S1**−OH formed under the same reaction conditions (**S1**−Cu^{I}/O_2 at 0 °C) at different reaction times (Figure 8B, right). Curiously, the reaction yields observed at short reaction times were very low (3−6% after 250 s) and increased gradually over time (>12% after 3000 s). The evolution of the reaction yields matched the kinetic traces obtained by UV−vis spectroscopy. It was concluded that, during the first oxidation process (gray spectra, 30 s), the C−H bond was still not oxidized. Moreover, it was observed that formation of the **S1**−OH product occurred during the formation and decay of the second intermediate species (evolution of the absorbance at 400 nm and product formation, Figure 8B).

Kinetic analysis of the reaction of **S1**−Cu^{I} with excess O_2 at 0 °C was carried out by varying the initial concentration of the Cu^{I} complex (1−4 mM). The reaction was followed by UV−vis, and the reaction rates for the different reaction steps were calculated by fitting the formation and decay curves to exponential functions (Figure 8C, also see the SI for further details). Changes in the absorbance at 620 nm correlate to the reaction rate for the first oxidation process (oxygenation, k_1), and the formation ("k_2") and decay ("k_3") of the second intermediate (brown spectra) were obtained by fitting the changes in absorbance at 400 nm (see the SI for further details). The traces could all be fit to first-order exponentials suggesting the involvement of mononuclear copper intermediates for each step (first-order dependence on Cu concentration, Figure 8C).[50]

The different intermediates observed by UV−vis (Figure 8A), the evolution of the hydroxylation product (Figure 8B), and the kinetic analysis of the reaction point toward the mechanism proposed in Figure 8. The oxygenation of LCu^{I} leads to a formation of the LCu^{II} complex (first intermediate), in which the C−H bond is not oxidized. It is the reaction of this LCu^{II} with H_2O_2 (generated by $O_2^{\bullet}$ disproportionation and/or acetone oxidation) that leads to C−H hydroxylation.[41,51,52] We postulate that the intramolecular C−H oxidation occurs via the formation of a mononuclear copper(II)-hydroperoxo complex (second intermediate, brown spectrum) that will decay to form the final C−OH product (green spectrum). The calculated rates have to be taken with caution. As previously stated, the formation of H_2O_2 occurs under substoichiometric conditions, which precludes accumulation of the putative LCu^{II}(OOH) intermediate: the concentration of LCu^{II}(OOH) is dependent on the concentration of H_2O_2; the calculated decomposition rate (k_3) is highly influenced by its formation rate (k_2, see the SI for further discussion). This issue will be bypassed in the next section by adding H_2O_2 under pseudo-first-order conditions (5−20 equiv).

Oxidation of S1−Cu^{I} with H_2O_2. The reactivity of **S1**−Cu^{I} with H_2O_2 was also followed by UV−vis under similar conditions. An acetone solution containing 20 equiv of H_2O_2 was added to the Cu^{I} complex (1 mM) under Ar at 0 °C, and the spectral changes were monitored for 3000 s (Figure 8D). In the presence of H_2O_2, the initial LCu^{I} species (orange spectrum) instantly changed to a new species (brown spectrum) with a high-energy transition at 370 nm (ε = 1800 M^{-1} cm^{-1}) and a shoulder at 470 nm (ε = 500 M^{-1} cm^{-1}). These spectral features are characteristic of LCu^{II}(OOH) species. These mononuclear intermediates are usually generated by the addition of H_2O_2 to LCu^{II} complexes in the presence of a base (NEt_3).[33,53−55] Karlin and co-workers have reported that the generation of a LCu^{II}(OOH) species can also be accomplished by the addition of 1.5 equiv of H_2O_2 to the corresponding LCu^{I} complex or alternatively by the LCu^{II}/H_2O_2/NEt_3 route.[55−57] The addition of 20 equiv of H_2O_2 to **S1**−Cu^{II} in the presence of 1 equiv of NEt_3 led to the generation of a fleeting species with UV−vis features that are identical to those obtained in the LCu^{I}/H_2O_2 reaction, suggesting the LCu^{II}(OOH) formulation.

The proposed [(**S1**)Cu^{II}(OOH)]$^{+}$ species thus observed decayed over time in a two-step fashion (Figure 8E). Rapid decay (300 s) was followed by a slower, second process (300−3000 s) that eventually led to the formation of a final species with a visible transition at 635 nm (green spectrum, Figure 8D). The hydroxylation yield reaction was also followed over the same time period (Figure 8E). At short reaction times (60 s), moderate reaction yields were observed (35%) that increase to 50−55% during the first 300 s. Similar to those for the oxidation of **S1**−Cu^{I}, these observations suggest that decay of the putative LCu^{II}(OOH) leads to the hydroxylation of the ligand scaffold (0−300 s). The second process (300−3000 s) is attributed to the slow decay of the Cu^{II} complex bearing the oxidized ligand scaffold, probably because of protonation.

Kinetic analysis of the reaction of **S1**−Cu^{I} with an excess of H_2O_2 at 0 °C was carried out by varying the initial concentration of the LCu^{I} complex (0.75−3.0 mM) and the concentration of H_2O_2 (5−20 mM). The generation of the putative LCu^{II}(OOH) intermediate was too fast to obtain its formation rate (5 s).[58] We propose that it occurs in a two-step fashion via a $1e^{-}$ oxidation of the initial Cu^{I} complex [LCu^{I} + $0.5H_2O_2$ = LCu^{II}(OH)] followed by a reaction of the resulting LCu^{II} complexes with 1 equiv of H_2O_2.[56] In fact, the full generation of LCu^{II}(OOH) from LCu^{I} was only accomplished when the reaction is carried out with amounts of H_2O_2 higher than 1.5 equiv (see the SI). From the decay of the LCu^{II}(OOH) (0−300 s), the rates of hydroxylation (k_3) could be calculated (Figure 8F). The reaction rates showed first-order dependence on LCu^{I} concentration and were independent of the H_2O_2 concentration. This kinetic behavior suggests the formation of mononuclear LCu^{II}(OOH) prior to the intramolecular hydroxylation step. A similar decay was observed when the proposed LCu^{II}(OOH) was generated by the LCu^{II}/H_2O_2/NEt_3 route (see the SI).

Oxidation of S2−Cu^{I} with O_2 and H_2O_2. The reactivity of **S2**−Cu^{I} toward O_2 and H_2O_2 was analyzed by UV−vis (Figure 9). In this case, we followed the reactions at −40 °C because of the higher reactivity of the steroid-derived complexes compared to that of the **S1** analogue; at 0 °C, the reactions with **S2**−Cu^{I} and oxidants were too fast to obtain kinetic data. Similar reaction intermediates were observed in the oxidation of **S2**−Cu^{I} with O_2 compared to those observed for **S1**−Cu^{I}. Two consecutive reaction steps led to the generation of the suggested LCu^{II}(OOH) (brown spectrum, Figure 9A), which

DOI: 10.1021/acs.joc.7b01069
J. Org. Chem. 2017, 82, 7887−7904

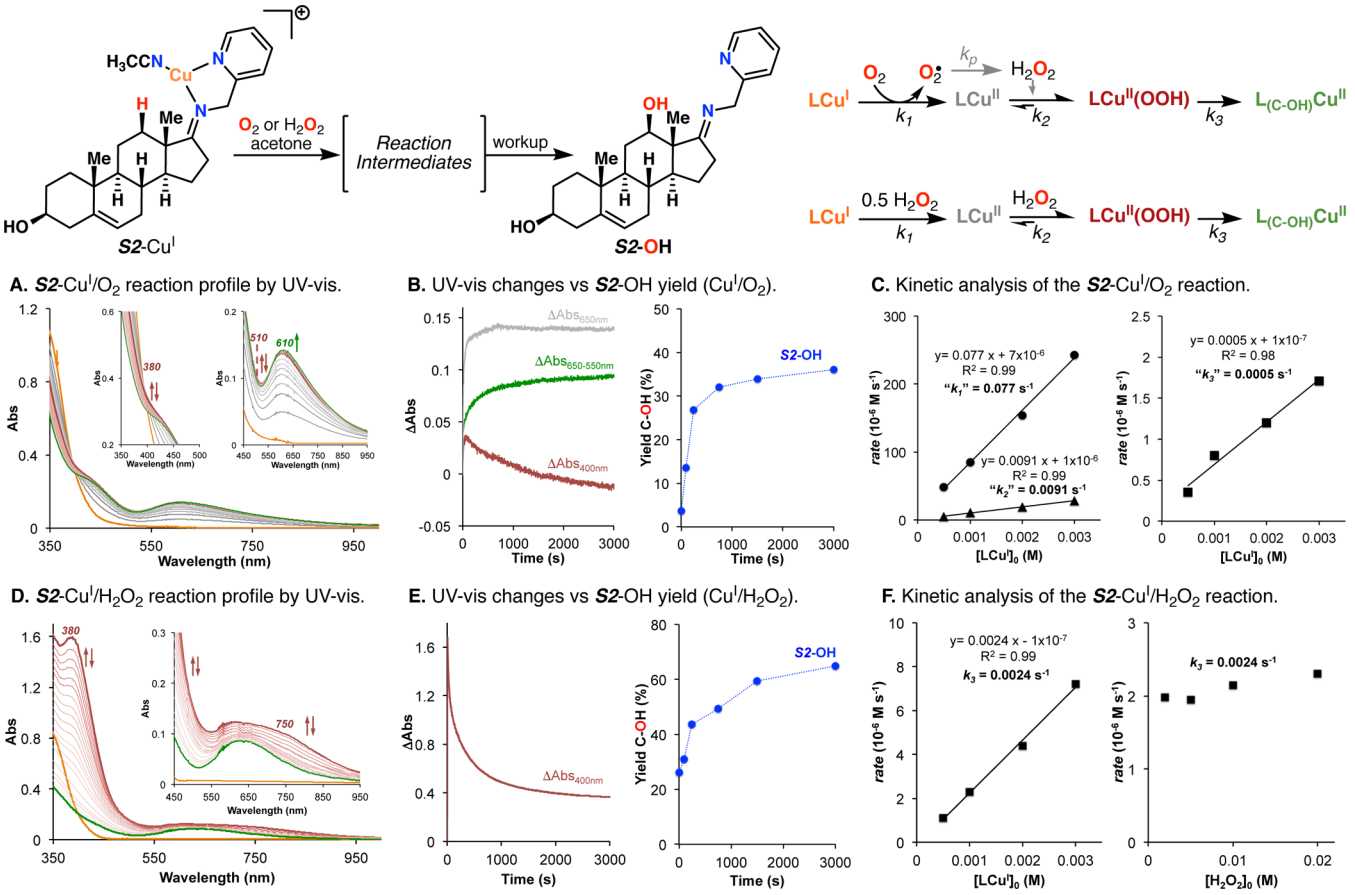

Figure 9. Oxidation of **S2**−Cu^I with O_2 or H_2O_2 at −40 °C. **S2**−Cu^I/O_2: (A) UV−vis spectral changes; (B) variation of the absorbance at selected wavelengths (left) and evolution of the reaction yield (**S2**−OH); (C) kinetic analysis. **S2**−Cu^I/H_2O_2: (D) UV−vis spectral changes; (E) variation of the absorbance at selected wavelengths (left) and evolution of the reaction yield (**S2**−OH); (F) kinetic analysis. It is noted that the evolution of the reaction yield was carried out at −40 °C ($[\mathbf{S2}-Cu^I]_0$ = 4 mM); the first quantification was done at t = 10 s. See text and the SI for details.

decayed to generate the final oxidation product (λ_{max} = 610−650 nm). The evolution of the reaction yields was also in agreement with the disappearance of the UV−vis features corresponding to the putative $LCu^{II}(OOH)$ intermediate (Figure 9B).

Upon variation of the Cu^I complex concentrations (0.5−3 mM; −40 °C, **S2**−Cu^I/O_2 in acetone), the apparent reaction rates for the formation of the proposed $LCu^{II}(OOH)$ intermediate ("k_1" and "k_2") and its decomposition ("k_3") were first-order-dependent on the initial concentration of LCu^I (Figure 9C). When compared with those for the oxidation of **S1**−Cu^I with O_2, the reaction rates obtained for the steroid-analogue complex were similar, even though the reactions were carried out at lower temperatures (0 versus −40 °C, respectively). Similar to those from before, the calculated reaction rates for the formation and decay of the $LCu^{II}(OOH)$ species have to be taken with caution because of their dependence on the rate of H_2O_2 generation (see the SI for detailed discussion).

The oxidation of **S2**−Cu^I with H_2O_2 was also followed by UV−vis at −40 °C (Figure 9D). The addition of excess of H_2O_2 (20 equiv) to a solution of the Cu^I complex (1 mM) under Ar led to the immediate formation of a putative $LCu^{II}(OOH)$ intermediate (λ_{max} = 380 nm, ε = 1600 M^{-1} cm^{-1}).[56] The same species was also independently generated by the addition of H_2O_2 to a solution containing **S2**−Cu^{II} and NEt_3. The decay of this $LCu^{II}(OOH)$ species was directly proportional to the evolution of the hydroxylation product (Figure 9E). The rate of the stepwise formation of the proposed $LCu^{II}(OOH)$ complex was too fast to measure (10 s), but we were able to calculate its decomposition rate by fitting the change in the absorbance at 400 nm to an exponential decay. The reaction rates showed first-order dependence on $[LCu^I]$ and were independent of $[H_2O_2]$, consistent with the proposed mechanism that suggests that the formation of the putative mononuclear $LCu^{II}(OOH)$ species occurs prior to the intramolecular hydroxylation of the ligand.

Reactivity with Other ROOH/ROOR Oxidants (R: tert-Butyl-, Cumyl-). The reactivity of **S1**−Cu^I toward other alkylhydroperoxo [*tert*-butyl hydroperoxide (*t*BuOOH) and dimethylbenzyl hydroperoxide (CumOOH)] and alkyl-peroxo [di-*tert*-butyl peroxide (*t*BuOO*t*Bu) and bis(1-methyl-1-phenylethyl) peroxide (CumOOCum)] oxidants was also evaluated (Figure 10).

The reaction of **S1**−Cu^I with *t*BuOOH (20 equiv) at 0 °C led to the immediate formation of a brown species (brown spectrum, Figure 10A). The spectral features of this intermediate (λ_{max} = 375 nm, ε = 1200 M^{-1} cm^{-1}) are similar to those of the putative $LCu^{II}(OOH)$ species but distinctive, and we formulate this new intermediate as the alkyl-peroxo complex $[(\mathbf{S1})Cu^{II}(OO\mathit{t}Bu)]^+$.[59] Analogous to that of the proposed $LCu^{II}(OOH)$ complex, its first-order decay led to the formation of the hydroxylation product. However, the half-life of the putative $LCu^{II}(OO\mathit{t}Bu)$ complex was significantly longer

DOI: 10.1021/acs.joc.7b01069
J. Org. Chem. 2017, 82, 7887−7904

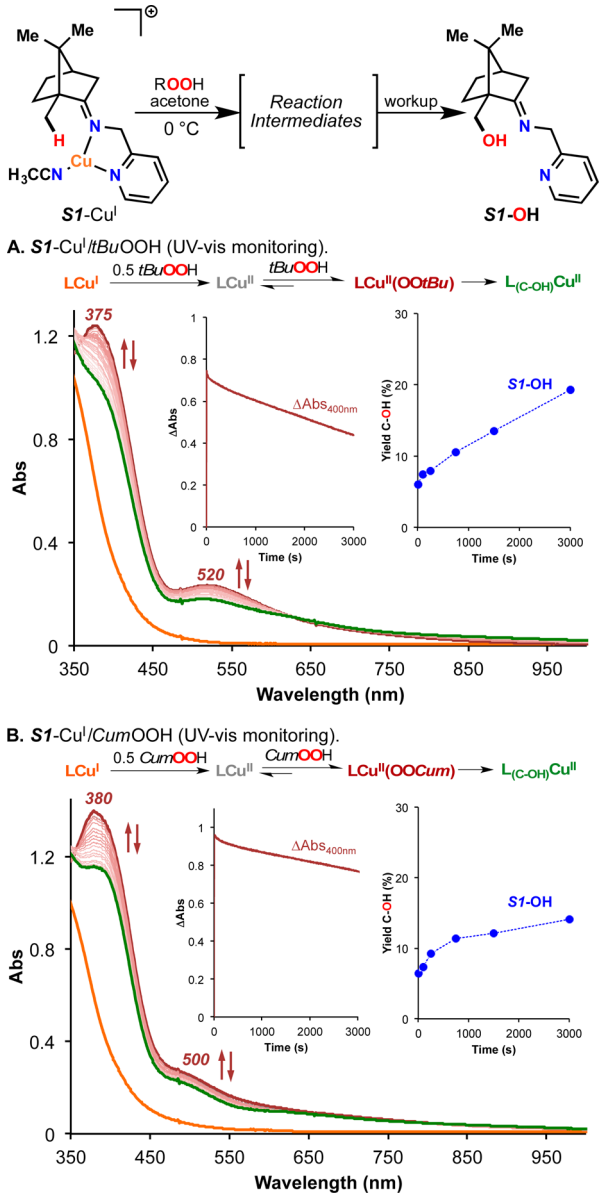

Figure 10. (A) Oxidation of **S1**−Cu^{I} with *t*BuOOH at 0 °C followed by UV−vis (inset, evolution of the absorbance and reaction yields). (B) Oxidation of **S1**−Cu^{I} with CumOOH at 0 °C followed by UV−vis (inset, evolution of the absorbance and reaction yields). See the SI for further details on kinetic analysis and the product quantification procedure.

(30 s versus 7 h), and its decomposition led to lower reaction yields (up to 18%). When exposed to *t*BuOO*t*Bu, **S1**−Cu^{I} was oxidized directly to a blue species without hydroxylation of the ligand (see the SI). This is a strong indication that the formation of the proposed $LCu^{II}(OOR)$ is required to oxidize the ligand scaffold.

In addition, the copper(II) cumyl-peroxo complex derived from the oxidation of **S1**−Cu^{I} with CumOOH was also studied (Figure 10B). In this case, the first-order decay of the proposed $[(\mathbf{S1})Cu^{II}(OOCum)]^{+}$ intermediate was even slower than that of the analogous *t*Bu complex ($t_{1/2}$, 14 h), and the decomposition was directly proportional to the hydroxylation of the **S1** scaffold, although low yields were obtained (up to 14% after 3000 s).[40,59] When the **S1**−Cu^{I} was exposed to CumOOCum, no hydroxylation product was observed. The above kinetic analysis supports the proposed mechanism, with the decay rates of the putative $[(\mathbf{S1})Cu^{II}(OOR)]^{+}$ species showing first-order dependence on LCu^{I} concentration and being independent of the ROOH concentration.

In a parallel study, the same methodology was used to generate the putative **S2**-derived alkyl-peroxo copper(II) complexes $[(\mathbf{S2})Cu^{II}(OOtBu)]^{+}$ and $[(\mathbf{S2})Cu^{II}(OOCum)]^{+}$ at −40 °C (see the SI). Their first-order decays were tied to the formation of the hydroxylation product, with the $[(\mathbf{S2})Cu^{II}(OOtBu)]^{+}$ complex being less stable than $[(\mathbf{S2})Cu^{II}(OOCum)]^{+}$ ($t_{1/2}$, 400 s versus 1800 s). In both cases, the decay of the proposed $LCu^{II}(OOR)$ complex led to lower yields than that of the $LCu^{II}(OOH)$ analogue (30−35% versus 60%). Kinetic analysis supports the proposed reaction mechanism, with the reaction rates calculated as independent of the initial concentrations of Cu^{I} and ROOH. When *t*BuOO*t*Bu and CumOOCum were used as the oxidants, no formation of Cu^{II}-alkylperoxo intermediate was observed, and in the analysis of the organic products derived from the oxidation, no hydroxylation product was observed (see the SI).

We also carried out the oxidation of **S1**−Cu^{I} and **S2**−Cu^{I} with acyl-hydroperoxides (*m*CPBA and peracetic acid). The reactivity was analogous to that of the reaction with *t*BuOO*t*Bu and CumOOCum; LCu^{II}-acylperoxo intermediates were not observed, and the ligand scaffold was not oxidized.

Additional Spectroscopic and Spectrometric Characterization of the Putative $LCu^{II}(OOR)$ Intermediates. For a further investigation into the mechanism, EPR measurements of the reaction intermediates and the final cupric products derived from the oxidation of **S1**−Cu^{I} with different oxidants were taken (see Figure S42). In agreement with the above-mentioned mechanistic proposal, the addition of O_2 to **S1**−Cu^{I} at 0 °C (EPR silent) led to the fast formation of mononuclear LCu^{II} intermediates with EPR signals characteristic of LCu^{II} complexes with a $d_{x^2-y^2}/d_{xy}$ ground state (e.g., square planar, square pyramidal)[5,55] and similar to the EPR spectra of the independently synthesized $[(\mathbf{S1})Cu^{II}(H_2O)_2(CF_3SO_3)]^{+}$ complex.

The EPR spectra of the various proposed $[(\mathbf{S1})Cu^{II}(OOR)]^{+}$ intermediates derived from the reaction between **S1**−Cu^{I} and ROOH oxidants (R: H-, *t*Bu-, and Cum-) were also studied. The addition of excess ROOH (20 mM) to cold solutions of **S1**−Cu^{I} (2 mM, 0 °C) led to the formation of $[(\mathbf{S1})Cu^{II}(OOR)]^{+}$ with similar ($g_{\parallel} > g_{\perp}$) but distinct ($2.33 > g_{\parallel} > 2.23$; see Figure S42) EPR features. The EPR spectrum of $[(\mathbf{S1})Cu^{II}(OOH)]^{+}$ generated from **S1**−Cu^{II}, H_2O_2, and NEt_3 (see Figure S44)[57] was also found to be similar to the one obtained in the reaction of **S1**−Cu^{I} with H_2O_2. Similar results were obtained in the oxidation of **S2**−Cu^{I} with O_2, H_2O_2, *t*BuOOH, and CumOOH at −40 °C (Figure S43).

In addition, the ESI-MS characterization of the products derived from the oxidation of the **S1**−Cu^{I} system with O_2, H_2O_2, *t*BuOOH, and CumOOH at 0 °C was attempted (see the SI). Unfortunately, the injection of cold solutions of the crude reaction did not lead to the detection of any of the $[(\mathbf{S1})Cu^{II}(OOR)]^{+}$ species. However, we were able to detect the final oxidation products (see Figure S45 in the SI). Labeling experiments using $^{16}O_2$ and $^{18}O_2$ showed that the oxygen atom incorporated in the **S1**−OH product was derived from O_2 reduction (**S1**−^{16}OH for $^{16}O_2$ and **S1**−^{18}OH for $^{18}O_2$, ^{18}O incorporation > 95%). Similar results were obtained when the oxidation was carried out with $H_2{}^{16}O_2$ or $H_2{}^{18}O_2$, suggesting that the oxidation products **S1**−^{16}OH or **S1**−^{18}OH (^{18}O

DOI: 10.1021/acs.joc.7b01069
J. Org. Chem. 2017, 82, 7887−7904

incorporation > 95%) are derived from the decay of the $[(\mathbf{S1})Cu^{II}(OOH)]^+$ intermediate.

O–O Cleavage Mechanism: Oxidation of External Substrates and Analysis of the Cumyl Radical Decay. Having identified the putative involvement of hydroperoxo copper(II) species in the observed C–H hydroxylation, we next seek experimental evidence for the nature of the O–O cleavage step. The analysis of the organic products derived from the O–O cleavage of metal-cumylperoxo species can be used to determine if the cleavage is heterolytic or homolytic in nature (Figure 11A).[60,61] If the CuO–OCum is broken heterolytically,

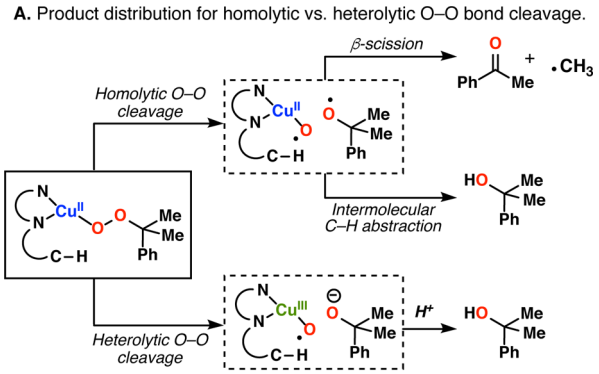

	Yield		
L = ***S1***, 20 °C	25%	28%	72%
0 °C	14%	17%	83%
–40 °C	8%	3%	97%
L = ***S2***, 20 °C	27%	26%	74%
0 °C	31%	7%	93%
–40 °C	36%	3%	96%

Figure 11. (A) Analysis of the $LCu^{II}(OOCum)$ decay products (CumOH vs acetophenone) as a mechanistic tool to determine the O–O cleavage mechanism (homo- vs heterolytic). (B) Products obtained in the decay of $[(\mathbf{S1})Cu^{II}(OOCum)]^+$ and $[(\mathbf{S2})Cu^{II}(OOCum)]^+$ at different temperatures.

$CumO^-$ would be generated and protonated to give cumyl alcohol. On the other hand, if the same species undergoes homolytic cleavage, $CumO^\bullet$ is formed and could either (1) undergo intramolecular $H^\bullet$ abstraction to give CumOH or (2) undergo β-scission to generate acetophenone.[40,62]

The decomposition products of the putative $LCu^{II}(OOCum)$ complexes at different temperatures were then analyzed for the amount of acetophenone, CumOH, and the oxidized ligand (by GC or ^1H NMR, see the SI for further details). In all cases, the formation of acetophenone was observed (ranging from 3% to 30%), in support of the homolytic O–O cleavage pathway (Figure 11B). Interestingly, the yield of the desired oxidation and the ratio of acetophenone to cumyl alcohol exhibited a marked temperature dependence. This could be accounted for by considering the rate of formation of $RO^\bullet$ and the lifetime of the radical (*vide infra*).

In all cases documented in the preceding sections, the trends in the yields of the oxidation using a different solvent (O_2, H_2O_2, *t*BuOOH, or CumOOH) could be explained from two perspectives. Within each substrate series (**S1** or **S2**), the amounts of hydroxylated products depend on the following: (1) the stability of the proposed intermediate $LCu^{II}(OOR)$ species (the less stable $LCu^{II}(OOR)$ species generally gave higher yields), and (2) the reactivity of the resulting radicals with the more reactive radical giving higher yields ($RO^\bullet$, see Figure 12). Between the two different substrate series studied,

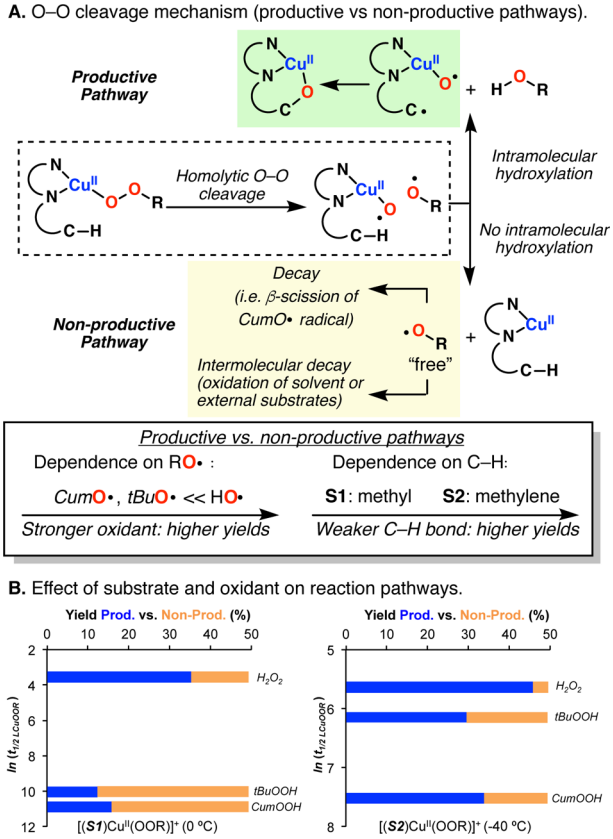

Figure 12. (A) Proposed O–O cleavage mechanism (homolytic) and fate of the $RO^\bullet$ species formed (intra- vs intermolecular decay). (B) Reaction yields measured after half-life decay of the putative $LCu^{II}(OOR)$ species for **S1** (left) and **S2** (right).

the yields could be rationalized on the basis of the strength of the oxidized C–H bond (bond dissociation free energy, BDFE). The consistently lower oxidation yields for **S1** relative to those of **S2** reflect the higher BDFE of primary C–H bonds (i.e., **S1**) to secondary C–H bonds (i.e., **S2**).

It is also worth mentioning that the decrease in the hydroxylation yield is greater for **S1** than for **S2** when oxidants other than H_2O_2 are used. This is clearly depicted in Figure 12B when plotting the half-life of the putative $LCu^{II}(OOR)$ species $[\ln(t_{1/2(LCuOOR)})]$ against the yields obtained at those reaction times. Ideally at 50% conversion, 50% of the hydroxylation product should be obtained if all the $RO^\bullet$ generated partakes in the intramolecular oxidation of the ligand after half of the $LCu^{II}(OOR)$ intermediate has decayed [time, half-life of $LCu^{II}(OOR)$]. Not surprisingly, the lowest yields were obtained for **S1** (primary C–H bond) in the presence of weaker $RO^\bullet$-abstracting reagents (*t*BuO$^\bullet$ and CumO$^\bullet$). To account for the fate of the $RO^\bullet$ species generated that led to nonproductive pathways, external substrates were added in excess (cyclohexane and 1,2-*cis*-dimethylcyclohexane, 1,2-*cis*-DMCH), which allowed quantification of the "escaped" O-centered radicals (Figure 13).

DOI: 10.1021/acs.joc.7b01069
J. Org. Chem. 2017, 82, 7887–7904

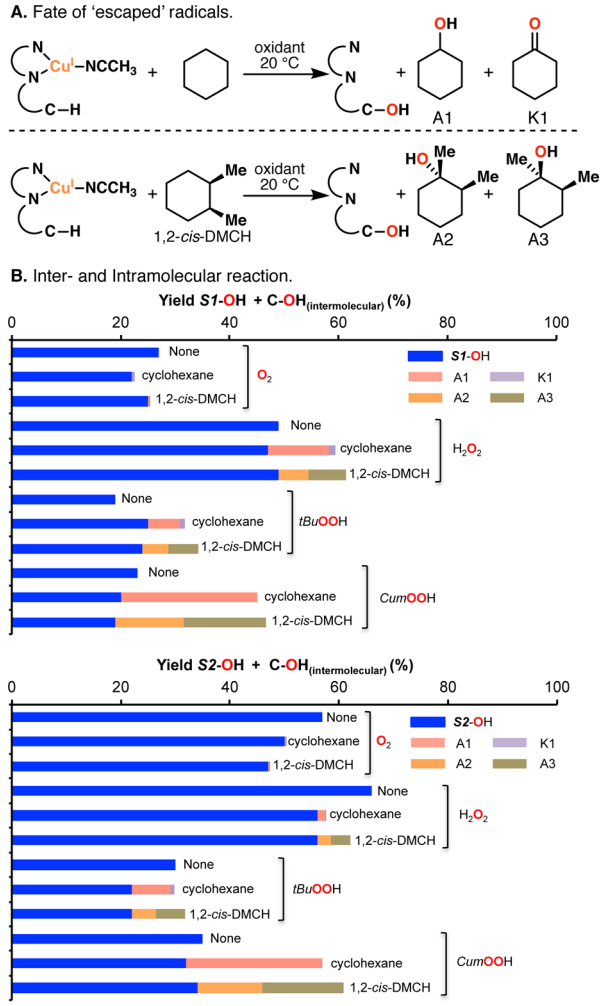

Figure 13. (A) Intermolecular oxidation experiments (substrates: cyclohexane and 1,2-*cis*-DMCH) carried out to quantify the free RO• species released after decay of the different $LCu^{II}(OOR)$ species (intramolecular products in blue). (B) Inter- vs intramolecular reaction. See the SI for further details.

In the cases where low hydroxylation yields were obtained (i.e., **S1** with *t*BuOOH and CumOOH), higher intermolecular oxidation yields were observed, which accounted for a higher percentage of RO• escaping the solvent cage. When the products of the intermolecular oxidation of 1,2-*cis*-DMCH were analyzed, equimolar mixtures of *cis*- and *trans*-hydroxylation products (A2 and A3) were found. This is characteristic of oxidations carried out by O-centered radicals (such as *t*BuO• and HO•), which lend further support for the proposed homolytic O−O cleavage of the putative $LCu^{II}(OOR)$ intermediate.[19,59,59]

When the results obtained with the different substrates (**S1** versus **S2**) with the same oxidant are compared, higher intermolecular oxidation yields were observed for **S1**. This is in agreement with **S1** being less prone to intramolecular hydroxylation than **S2**. The results obtained with O_2 are also consistent with H_2O_2 being the active oxidant: like in the oxidation with H_2O_2, low intermolecular oxidation yields were obtained, suggesting that the formed O-centered radical (•OH) is highly selective toward intramolecular oxidation. Importantly, the overall combined oxidation yield (inter- and intramolecular) of these reactions (LCu^{I} with O_2 or H_2O_2) increased with the yield of the desired intramolecular hydroxylation which suggests that oxidation of the ligand occurs within the solvent cage and that the efficiency of the reaction is dependent on the rate of diffusion of the hydroxyl radicals from the solvent cage (i.e., higher diffusion in the oxidation of **S1**).

Radical Traps: Halogenated Cosolvents. Following the initial H• abstraction by the different RO• species, a C-centered radical is formed, which was proposed to rebound to the proximal Cu^{II}−O• center to give the final C−O bond (see Figures 6 and 14). In order to detect the putative C-centered radical, the oxidation of **S1**−Cu^{I} and **S2**−Cu^{I} with different oxidants (O_2, H_2O_2, *t*BuOOH, and CumOOH) was carried out in the presence of the halogenated solvents (CCl_3Br and CCl_4). These cosolvents would serve as a radical trap as they could suffer an attack from the C-centered radicals to form C−halogen bonds, with CCl_3Br being more prone to halogen-radical formation than CCl_4 ($BDFE_{(C-Br)} < BDFE_{(C-Cl)}$).

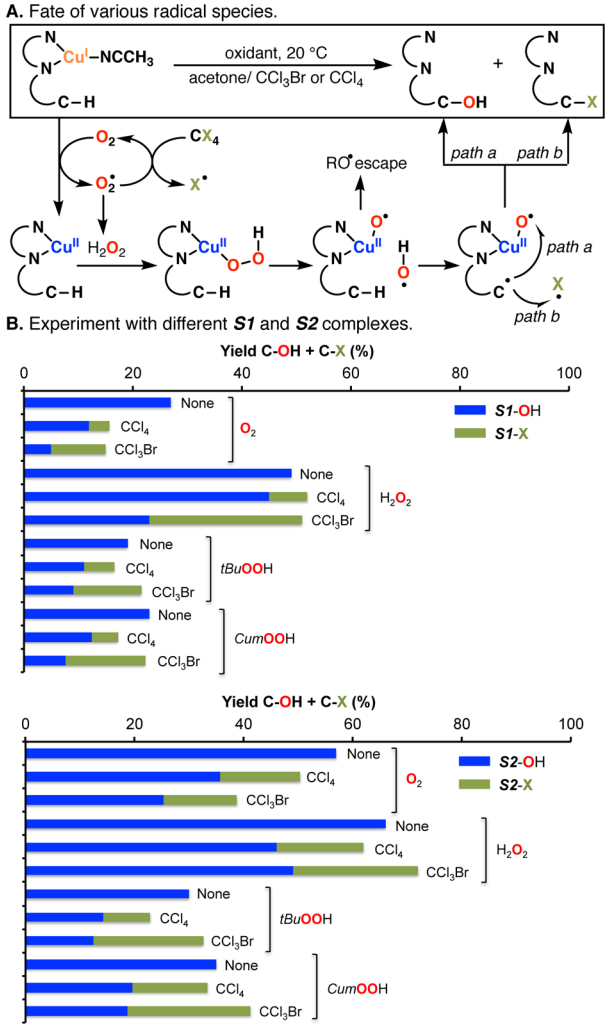

Figure 14. Radical trapping experiment. (A) Fate of various radical species. (B) Reaction of **S1**−Cu^{I} and **S2**−Cu^{I} with different oxidants at 20 °C (O_2, H_2O_2, *t*BuOOH, and CumOOH) in the presence of radical trap reagents CCl_4 and CCl_3Br (^1H NMR yields, see the SI for details).

As shown in Figure 14, the formation of the halogenated products (halogen, Cl and Br) was observed in all reactions albeit in varying degrees. When O_2 was used as the oxidant,

DOI: 10.1021/acs.joc.7b01069
J. Org. Chem. 2017, 82, 7887−7904

significant suppression in the overall oxidation yields (C−OH + C−X) was observed with a 20−50% decrease (Figure 14B). We postulate that, in the presence of CCl_3Br or CCl_4, the initially formed O-centered radical species (i.e., superoxide from the reaction of LCu^I with O_2), which would be necessary for H_2O_2 generation, suffered from partial quenching. This would result in a tempered rate and quantity of H_2O_2 formation which lead to lower oxidation yields.

Similar to the results obtained in the intermolecular oxidations (see Figure 13), a higher degree of halogenation for the **S1** complex than that for **S2** was observed when using H_2O_2 as the oxidant. This is in agreement with the fact that in **S1** the oxidized C−H bond has a higher BDFE than that in **S2** (CH_3 versus CH_2), which leads to greater amounts of RO• escaping the solvent cage and reacting with the halogenated solvent (RO• escape pathway in Figure 14). Across the various oxidants, higher degrees of halogenation (C−X versus C−O) were observed when poorer oxidants were employed: the lower oxidizing abilities of CumO• and *t*BuO• result in a higher degree of the nonproductive pathway (RO• escape).

Applying the Mechanistic Findings To Improve the Previous Oxidation Methodology. Inspired by the new mechanistic proposal, we decided to redesign the oxidative reaction conditions with the main objective of finding a more convenient Cu source and oxidant. Consequently, a reinvestigation of the conditions with 2-picolylimine of dehydro-*epi*-androsterone (**S2**) was carried out. A representative optimization table is presented in Figure 15A. Although $Cu(OTf)_2$ was used in all the above-mentioned mechanistic studies, $Cu^{II}(NO_3)_2{\cdot}3H_2O$ was found experimentally to be the best source of Cu^{II}, showing comparable if not better reactivity, and also to be more economical. Notably, other sources of Cu^{II} showed severely diminished reactivity (see the SI for details).

In accordance to our proposed mechanism, hydrogen peroxide proved to be the best oxidant. In addition, the usage of the imine derived from commercial 2-picolylamine gave comparable yields to the 4-methyl derivative. Combined with a solvent change from acetone to THF, full consumption of the starting material could be effected at room temperature in 60 min, providing the product in excellent NMR and isolated yields. Finally, we were able to eliminate the use of the reductant (i.e., benzoin or sodium ascorbate), and the current protocol exhibits good tolerance to moisture and oxygen (open-flask reaction setup).

A representative scope of the new protocol is shown in Figure 15B. A survey of different steroidal substrates with the new reaction conditions gave the desired hydroxylated products in good-to-excellent yields (70−93%). A gram-scale example was also included with comparable efficiency delivering **P2** in high yields (1.22 g, 80%). Of note, all these reactions were run open to air without any special precautions in both reagent storage and experimental setup. We would like to point out that the oxidation of the steroid substrates is stereospecific despite the fact that the oxidation occurs via H-atom abstraction by RO• radical species. The orientation of the Cu(II)-oxyl species and the rigidity of the steroid scaffold could only accommodate a single conformation during the stereodetermining rebound step during C−O bond formation.

For the camphor-imine substrate, the hydroxylation product was obtained in good yields (81% NMR yield and 74% isolated yield) with slight modification to the reaction conditions. These results are superior to the yields obtained by Schönecker (Cond. I, 31%; Cond. II, 4%) and comparable with the yields

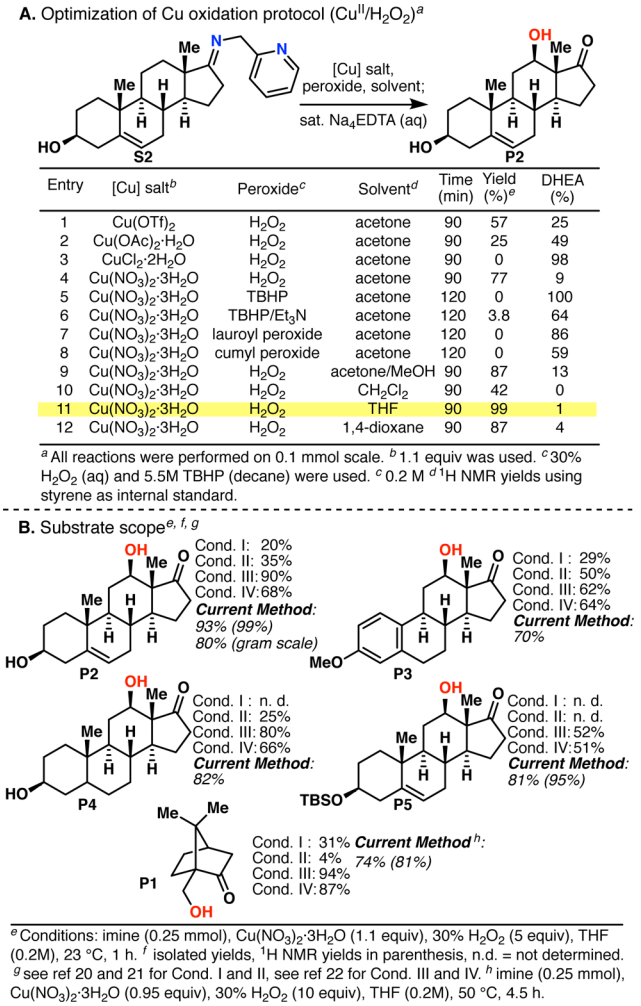

Entry	[Cu] salt[b]	Peroxide[c]	Solvent[d]	Time (min)	Yield (%)[e]	DHEA (%)
1	$Cu(OTf)_2$	H_2O_2	acetone	90	57	25
2	$Cu(OAc)_2{\cdot}H_2O$	H_2O_2	acetone	90	25	49
3	$CuCl_2{\cdot}2H_2O$	H_2O_2	acetone	90	0	98
4	$Cu(NO_3)_2{\cdot}3H_2O$	H_2O_2	acetone	90	77	9
5	$Cu(NO_3)_2{\cdot}3H_2O$	TBHP	acetone	120	0	100
6	$Cu(NO_3)_2{\cdot}3H_2O$	TBHP/Et_3N	acetone	120	3.8	64
7	$Cu(NO_3)_2{\cdot}3H_2O$	lauroyl peroxide	acetone	120	0	86
8	$Cu(NO_3)_2{\cdot}3H_2O$	cumyl peroxide	acetone	120	0	59
9	$Cu(NO_3)_2{\cdot}3H_2O$	H_2O_2	acetone/MeOH	90	87	13
10	$Cu(NO_3)_2{\cdot}3H_2O$	H_2O_2	CH_2Cl_2	90	42	0
11	$Cu(NO_3)_2{\cdot}3H_2O$	H_2O_2	THF	90	99	1
12	$Cu(NO_3)_2{\cdot}3H_2O$	H_2O_2	1,4-dioxane	90	87	4

[a] All reactions were performed on 0.1 mmol scale. [b] 1.1 equiv was used. [c] 30% H_2O_2 (aq) and 5.5M TBHP (decane) were used. [c] 0.2 M [d] ^1H NMR yields using styrene as internal standard.

[e] Conditions: imine (0.25 mmol), $Cu(NO_3)_2{\cdot}3H_2O$ (1.1 equiv), 30% H_2O_2 (5 equiv), THF (0.2M), 23 °C, 1 h. [f] isolated yields, ^1H NMR yields in parenthesis, n.d. = not determined. [g] see ref 20 and 21 for Cond. I and II, see ref 22 for Cond. III and IV. [h] imine (0.25 mmol), $Cu(NO_3)_2{\cdot}3H_2O$ (0.95 equiv), 30% H_2O_2 (10 equiv), THF (0.2M), 50 °C, 4.5 h.

Figure 15. New oxidation protocol (Cu^{II}/H_2O_2) for the directed oxidation of various substrates and comparison of its performance to the previous methodology.[16−18,22] See the SI for further details.

found using Baran's methods (Cond. III, 94%; Cond. IV, 87%). It is worth mentioning that, with these reaction conditions, we were able to reduce the amount of Cu used (0.95 versus 2.3 equiv), decrease the reaction times (4.5 versus 6 h), and avoid the use of a reductant (0 versus 2.3 equiv of ascorbate).

■ OUTLOOK AND CONCLUSIONS

In this article, we reported our detailed studies on the mechanism of the hydroxylation of substrate-containing imino-pyridine ligands with copper under various oxidative conditions. To our knowledge, this is the most comprehensive mechanistic study of Cu-directed C−H oxygenation to date. First, we isolated and characterized the LCu^I and LCu^{II} complexes bearing either one or two substrate-containing ligands. With these isolated crystalline complexes, their reactivities under different conditions (e.g., different solvents, temperatures, and oxidants) were investigated. We observed that, in the oxygenation of the Cu^I complexes, the reaction yield was temperature-dependent, surpassing the 50% threshold at high temperatures (50 °C). These results led us to reconsider the previous mechanistic proposal, which suggested that Cu_2O_2 intermediates [i.e., $Cu^{II}_2(O_2^{2-})$ and $Cu^{III}_2(O^{2-})_2$] were involved in the intramolecular C−H hydroxylation. Instead, we provided extensive experimental evidence for a new

DOI: 10.1021/acs.joc.7b01069
J. Org. Chem. 2017, 82, 7887−7904

mechanistic scenario in which the copper-mediated oxidation occurs via a mononuclear monooxygenase-type fashion similar to the oxidative pathways proposed for some copper-dependent monooxygenase enzymes (i.e., PHM and LPMO).

In the *first reaction step*, the Cu^{I} complexes react with O_2 to generate Cu^{II} and superoxide, which further reacts to form H_2O_2 (by disproportionation and oxidation of the solvent). We detected and quantified the products derived from the oxidation of the solvent, showing that at high temperatures the solvent provides the electrons that are necessary to overcome the 50% yield threshold.

In the *second reaction step*, Cu^{II} reacts with H_2O_2, which were generated in situ, leading to the formation of putative $LCu^{II}(OOH)$ intermediates.[63] Kinetic analysis of the reaction between Cu^{I} and O_2 revealed a multistep reaction, with the initial formation of Cu^{II} followed by the generation of the mononuclear $LCu^{II}(OOH)$ species. We were also able to independently generate these proposed $LCu^{II}(OOH)$ species by the reaction of Cu^{I} (or Cu^{II} + base) with H_2O_2; these species were characterized by different spectroscopic means (i.e., UV−vis and EPR).

In the *third reaction step*, the fleeting $LCu^{II}(OOH)$ intermediate undergoes homolytic O−O cleavage, to generate O-centered species (i.e., hydroxyl radical). We used various ROOH oxidants (H_2O_2, *t*BuOOH, and CumOOH) to demonstrate that, after the formation of the suggested $LCu^{II}(OOR)$ intermediates, homolytic O−O bond cleavage occurs to generate $RO^{\bullet}$ species (by analyzing the $CumO^{\bullet}$ decay and by trapping the $RO^{\bullet}$ formed with external substrates).

In the *fourth reaction step*, the $RO^{\bullet}$ generated will abstract a $H^{\bullet}$ atom from the ligand scaffold to generate a carbon-centered radical before intramolecular C−O bond formation. In the presence of halogenated solvents (CCl_4 and CCl_3Br), we observed the formation of C−Cl and C−Br products generated in the reaction between the C-centered radical species and the halogen sources.

Inspired by the mechanistic findings, we simplified the experimental protocol. In the new method, we made use of stoichiometric amounts of inexpensive Cu^{II} and an excess of H_2O_2 to oxidize substrates with excellent yields (70−99%). These new reaction conditions improved the previous methodologies in terms of practicability (no O_2 required and reactions at room temperature in an open flask), cost (use of Cu^{II} instead of Cu^{I} sources and no addition of external reductants), and yield.

Our present work is focused on obtaining detailed structural, spectroscopic, spectrometric, and computational characterization of the proposed mononuclear $LCu^{II}(OOR)$ species and on applying the lessons learned through this mechanistic study in a more general context, such as in the directed site selective oxidation of other aliphatic and unsaturated C−H bonds. The mechanistic insights into the Cu-directed hydroxylation reaction described herein could pave the way to fine-tune the oxidative properties of Cu-based iminopyridine systems, thereby enabling the development of powerful new catalysts for C−H oxidation.

EXPERIMENTAL SECTION

Materials. All reagents and solvents were purchased at the highest level of purity and used as received except as noted. Solvents were purified and dried by passing through an activated alumina purification system (INERT Pure Solv) or by conventional distillation techniques. All the substrate−imine−pyridine systems (**S1**−**S3**) were synthesized as previously reported.[22]

Physical Methods. Syntheses of copper(I) and copper(II) complexes were carried out under anaerobic conditions in an Inert I-LAB Glovebox system. UV−vis measurements were carried out by using a Hewlett-Packard 8454 diode array spectrophotometer with a 10 mm path quartz cell. The spectrometer was equipped with HP Chemstation software and a Unisoku cryostat for low-temperature experiments. NMR spectra were recorded in 7 in., 5 mm o.d. NMR tubes on a JEOL 500 MHz spectrometer in the Department of Chemistry at Southern Methodist University. GC analyses were performed on a Thermo Fisher TRACE 1300 (Chirasil-DEX column, 25 m). The products were identified by the comparison of their GC retention times with those of commercial samples. ESI-MS spectrometry was performed at the Shimadzu Center for Advanced Analytical Chemistry at the University of Texas, Arlington. ESI-MS spectra of the reaction intermediates generated *in situ* were acquired using a Finnigan LCQ Duo ion-trap mass spectrometer equipped with an electrospray ionization source (Thermo Finnigan, San Jose, CA). Elemental analysis (Elem Anal.) was performed by the ALS Group USA, Corp. doing business as ALS Environmental (Tucson, Arizona). For single crystal X-ray crystallography, all reflection intensities were measured at 110(2) K using a SuperNova diffractometer (equipped with Atlas detector) with Cu Kα radiation (λ = 1.541 78 Å) under the program CrysAlisPro (version 1.171.36.32 Agilent Technologies, 2013). The temperature of the data collection was controlled using the system Cryojet (manufactured by Oxford Instruments). Electron paramagnetic resonance (EPR) spectra were recorded on a Bruker EMX spectrometer controlled with a Bruker ER 041 X G microwave bridge operating at X-band (~9.4 GHz). All NMR spectra were recorded in 7 in., 5 mm o.d. NMR tubes.

Synthesis of Copper Complexes. The synthesis of the copper complexes was carried out in the glovebox and with the use of distilled acetone.

For the synthesis of **S1**−Cu^{I}, **S1** (100 mg, 0.41 mmol) was dissolved in acetone (1 mL) in a 20 mL vial equipped with a stir bar. $[Cu^{I}(CH_3CN)_4](PF_6)$ (160 mg, 0.41 mmol) was added to the ligand solution. After 30 min, Et_2O (20 mL) was added to precipitate the complex as a yellow powder (175 mg, 87% yield). The resulting solid was recrystallized in acetone/Et_2O, leading to yellow crystals. ^{1}H NMR (acetone-d_6): 8.59 (m, 1H, Py−*H*), 8.00 (m, 1H, Py−*H*), 7.57 (m, 1H, Py−*H*), 7.51 (m, 1H, Py−*H*), 4.93 (d, 1H, NC*H*$_2$Py), 4.89 (d, 1H, NC*H*$_2$Py), 2.81 (d, 1H, C−H), 2.37 (s, 3H, Cu−NCC*H*$_3$), 2.31 (d, 1H, C−H), 2.05 (m, 1H, C−H), 1.92 (m, 1H, C−H), 1.77 (m, 1H, C−H), 1.43 (m, 1H, C−H), 1.32 (m, 1H, C−H), 1.29 (s, 3H, C−H$_3$), 0.95 (s, 3H, C−H$_3$), 0.78 (s, 3H, C−H$_3$). Elem Anal. Calcd for $C_{18}H_{25}CuF_6N_3P\cdot0.2H_2O$: C, 43.6%; H, 5.2%; N, 8.5%. Found: C, 43.3%; H, 5.0%; N, 8.5%. ESI-MS (*m*/*z*): 346.1 $[M - PF_6]^+$.

For the synthesis of **S1**$_2$−Cu^{I}, **S1** (100 mg, 0.41 mmol) was dissolved in acetone (1 mL) in a 20 mL vial equipped with a stir bar. $[Cu^{I}(CH_3CN)_4](PF_6)$ (80 mg, 0.205 mmol) was added to the ligand solution. After 30 min, Et_2O (20 mL) was added in order to precipitate the complex as an intense yellow powder (122 mg, 88% yield). The resulting solid was recrystallized in acetone/Et_2O, leading to intense yellow crystals. ^{1}H NMR (acetone-d_6): 8.35 (m, 1H, Py−*H*), 7.92 (m, 1H, Py−*H*), 7.55 (m, 1H, Py−*H*), 7.49 (m, 1H, Py−*H*), 5.01 (d, 1H, NC*H*$_2$Py), 4.95 (d, 1H, NC*H*$_2$Py), 2.76 (d, 1H, C−*H*), 2.28 (d, 1H, C−*H*), 2.05 (m, 1H, C−*H*), 1.88 (m, 1H, C−*H*), 1.59 (m, 1H, C−*H*), 1.32 (m, 2H, C−*H*), 1.32 (m, 1H, C−*H*), 1.07 (s, 3H, C−*H*$_3$), 0.88 (s, 3H, C−*H*$_3$), 0.79 (s, 3H, C−*H*$_3$). Elem Anal. Calcd for $C_{32}H_{44}CuF_6N_4P\cdot0.2CH_3CN$: C, 55.5%; H, 6.4%; N, 8.4%. Found: C, 55.1%; H, 6.8%; N, 8.9%. ESI-MS (*m*/*z*): 547.3 $[M - PF_6]^+$.

For the synthesis of **S1**−Cu^{II}, **S1** (50 mg, 0.21 mmol) was dissolved in acetone (1.5 mL) in a 20 mL vial equipped with a stir bar. $Cu^{II}(CF_3SO_3)_2$ (77 mg, 0.21 mmol) was added to the ligand solution which turned intensely green. After 30 min, Et_2O (20 mL) was added. After 30 min, a green precipitate was separated (40 mg), and a blue filtrate was transferred into another 20 mL vial. After 5 days, blue crystals were isolated from the filtrate solution (62 mg, 46% yield). Elem Anal. Calcd for $C_{18}H_{26}CuF_6N_2O_8S_2$: C, 33.8%; H, 4.1%; N,

DOI: 10.1021/acs.joc.7b01069
J. Org. Chem. 2017, 82, 7887−7904

4.4%. Found: C, 34.2%; H, 4.5%; N, 4.4%. ESI-MS (m/z): 454.1 [M − CF_3SO_3 − $2H_2O$]$^+$.

For the synthesis of **S1**$_2$−Cu^{II}, **S1** (100 mg, 0.41 mmol) was dissolved in acetone (1.5 mL) in a 20 mL vial equipped with a stir bar. Cu^{II}(CF_3SO_3)$_2$ (77 mg, 0.205 mmol) was added to the ligand solution causing the solution to turn intensely green. After 30 min, Et_2O (20 mL) was added to precipitate the complex as a green powder (154 mg, 89% yield). The resulting solid was recrystallized using an acetone/Et_2O mixture, leading to green crystals. Elem Anal. Calcd for $C_{34}H_{44}CuF_6N_4O_6S_2·2H_2O$: C, 46.3%; H, 5.5%; N, 6.4%. Found: C, 46.1%; H, 5.4%; N, 6.7%. ESI-MS (m/z): 547.2 [M − $2CF_3SO_3$]$^+$.

For the synthesis of **S2**—Cu^{I}, **S2** (55 mg, 0.145 mmol) was suspended in acetone (1 mL) in a 10 mL vial equipped with a stir bar. [Cu^{I}(CH_3CN)$_4$](PF_6) (56 mg, 0.145 mmol) was added to the ligand solution. After 30 min, Et_2O (20 mL) was added to precipitate the complex as a colorless powder (80 mg, 88% yield). ^{1}H NMR (acetone-d_6): 8.59 (m, 1H, Py—H), 8.01 (m, 1H, Py—H), 7.59 (m, 1H, Py—H), 7.52 (m, 1H, Py—H), 5.33 (m, 1H, C═CH), 4.93 (m, 2H, NCH_2Py), 3.64 (bs, 1H, O—H), 3.36 (m, 1H, C—H), 2.82 (m, 2H, C—H), 2.61 (m, 2H, C—H), 2.41 (s, 3H, Cu—CH_3CN), 2.20—1.90 (m, 3H, C—H), 1.80−1.30 (m, 10H, C—H), 1.10−0.90 (m, 8H, C—H). Elem Anal. Calcd for $C_{27}H_{37}CuF_6N_3OP·0.5H_2O$: C, 50.9%; H, 6.0%; N, 6.6%. Found: C, 50.7%; H, 6.0%; N, 6.6%. ESI-MS (m/z): 589.2 [M − CH_3CN]$^+$.

For the synthesis of **S2**$_2$—Cu^{I}, **S2** (110 mg, 0.29 mmol) was suspended in acetone (1 mL) in a 10 mL vial equipped with a stir bar. [Cu^{I}(CH_3CN)$_4$](PF_6) (56 mg, 0.145 mmol) was added to the ligand solution. After 30 min, Et_2O (20 mL) was added to precipitate the complex as a yellow powder (140 mg, 99% yield). The resulting solid was recrystallized in an acetone/Et_2O mixture, leading to yellow crystals. ^{1}H NMR (acetone-d_6): 8.31 (m, 2H, Py—H), 7.95 (m, 2H, Py—H), 7.59 (m, 2H, Py—H), 7.41 (m, 2H, Py—H), 5.31 (m, 2H, C═CH), 4.99 (m, 4H, NCH_2Py), 3.63 (bs, 2H, O—H), 3.34 (m, 2H, C—H), 2.82 (m, 4H, C—H), 2.33 (m, 2H, C—H), 2.30−1.90 (m, 8H, C—H), 1.80−1.20 (m, 20H, C—H), 1.10−0.80 (m, 14H, C—H). Elem Anal. Calcd for $C_{18}H_{25}CuF_6N_3P·H_2O$·acetone: C, 61.1%; H, 7.3%; N, 5.4%. Found: C, 61.3%; H, 7.0%; N, 5.1%. ESI-MS (m/z): 819.5 [M − PF_6]$^+$.

For the synthesis of **S2**−Cu^{II}, **S2** (76 mg, 0.2 mmol) was suspended in acetone (1 mL) in a 10 mL vial equipped with a stir bar. Cu^{II}(CF_3SO_3)$_2$ (73 mg, 0.145 mmol) was added to the ligand solution. After 30 min, Et_2O (20 mL) was added to precipitate the complex as a blue powder (120 mg, 77% yield). Elem Anal. Calcd for $C_{18}H_{25}CuF_6N_3P·H_2O$·acetone: C, 61.1%; H, 7.3%; N, 5.4%. Found: C, 61.3%; H, 7.0%; N, 5.1%. ESI-MS (m/z): 590.1 [M − CF_3SO_3 − $2H_2O$]$^+$.

For the synthesis of **S2**$_2$−Cu^{II}, **S2** (76 mg, 0.2 mmol) was suspended in acetone (1 mL) in a 10 mL vial equipped with a stir bar. Cu^{II}(CF_3SO_3)$_2$ (37 mg, 0.1 mmol) was added to the ligand solution. After 30 min, Et_2O (20 mL) was added to precipitate the complex as a green powder (110 mg, 99% yield). Elem Anal. Calcd for $C_{52}H_{68}CuF_6N_4O_8S_2·H_2O$: C, 54.9%; H, 6.2%; N, 4.9%. Found: C, 54.4%; H, 6.3%; N, 4.9%. ESI-MS (m/z): 819.5 [M − $2CF_3SO_3$]$^+$.

For the synthesis of **S3**−Me−Cu^{I}, **S3**−Me (80 mg, 0.2 mmol) was suspended in acetone (1 mL) in a 10 mL vial equipped with a stir bar. [Cu^{I}(CH_3CN)$_4$](PF_6) (75 mg, 0.1 mmol) was added to the ligand solution. After 30 min, Et_2O (20 mL) was added to precipitate the complex as a white powder (140 mg, 99% yield). The resulting solid was recrystallized in an acetone/Et_2O mixture, leading to pale yellow crystals. ^{1}H NMR (acetone-d_6): 8.44 (bs, 1H, Py−H), 7.42 (bs, 1H, Py−H), 7.35 (bs, 1H, Py−H), 4.85 (m, 2H, NCH_2Py), 3.46 (m, 2H, C−H), 2.82 (m, 2H, C−H), 2.61 (m, 1H, C−H), 2.50 (bs, 1H, O−H), 2.41 (s, 3H, Cu−CH_3CN), 2.38 (s, 3H, Py−CH_3), 1.95 (m, 1H, C−H), 1.80−1.50 (m, 7H, C−H), 1.40−1.20 (m, 7H, C−H), 1.10 (m, 1H, C−H), 0.98 (m, 1H, C−H), 0.95 (s, 3H, C−H_3), 0.85 (s, 3H, C−H_3), 0.7 (s, 1H, C−H). Elem Anal. Calcd for $C_{28}H_{41}CuF_6N_3OP·H_2O$: C, 50.8%; H, 6.5%; N, 6.3%. Found: C, 51.2%; H, 6.8%; N, 6.0%. ESI-MS (m/z): 515.3 [M − PF_6 + $(CH_3)_2CO$]$^+$.

For the synthesis of **S3**−Me$_2$−Cu^{I}, **S3**−Me (50 mg, 0.13 mmol) was suspended in acetone (1 mL) in a 10 mL vial equipped with a stir bar. [Cu^{I}(CH_3CN)$_4$](PF_6) (24 mg, 0.065 mmol) was added to the ligand solution. After 30 min, Et_2O (20 mL) was added to precipitate the complex as a yellow powder (55 mg, 85% yield). ^{1}H NMR (acetone-d_6): 8.16 (bs, 2H, Py−H), 7.38 (bs, 2H, Py−H), 7.24 (bs, 2H, Py−H), 4.88 (bs, 4H, NCH_2Py), 3.46 (m, 4H, C−H), 2.80 (m, 4H, C−H), 2.50 (m, 2H, C−H), 2.40 (s, 6H, Py-CH_3), 2.30 (bs, 2H, O−H), 1.95 (m, 2H, C−H), 1.80−1.40 (m, 14H, C−H), 1.40−1.00 (m, 14H, C−H), 1.00−0.69 (m, 16H, C−H). Elem Anal. Calcd for $C_{52}H_{76}CuF_6N_4O_2P·3H_2O$: C, 59.2%; H, 7.7%; N, 5.4%. Found: C, 58.7%; H, 7.2%; N, 5.7%. ESI-MS (m/z): 851.5 [M − PF_6]$^+$.

For the synthesis of **S3**−Me−Cu^{II}, **S3**−Me (50 mg, 0.13 mmol) was suspended in acetone (1 mL) in a 10 mL vial equipped with a stir bar. Cu^{II}(CF_3SO_3)$_2$ (47 mg, 0.13 mmol) was added to the solution. After 30 min, Et_2O (20 mL) was added to precipitate the complex as a pale blue powder (75 mg, 75% yield). Elem Anal. Calcd for $C_{28}H_{42}CuF_6N_2O_9S_2$: C, 42.5%; H, 5.3%; N, 3.5%. Found: C, 42.5%; H, 5.5%; N, 3.9%. ESI-MS (m/z): 606.2 [M − CF_3SO_3 − $2H_2O$]$^+$.

For the synthesis of **S3**−Me$_2$−Cu^{II}, **S3**−Me (50 mg, 0.13 mmol) was suspended in acetone (1 mL) in a 10 mL vial equipped with a stir bar. Cu^{II}(CF_3SO_3)$_2$ (23 mg, 0.065 mmol) was added to the ligand solution. After 30 min, Et_2O (20 mL) was added to precipitate the complex as a pale green powder (60 mg, 80% yield). Elem Anal. Calcd for $C_{54}H_{76}CuF_6N_4O_8S_2·1.5H_2O$: C, 55.0%; H, 6.8%; N, 4.8%. Found: C, 54.5%; H, 6.8%; N, 5.3%. ESI-MS (m/z): 851.5 [M − $2CF_3SO_3$]$^+$.

For the synthesis of **S3**−Cu^{I}, **S3** (53 mg, 0.14 mmol) was suspended in acetone (1 mL) in a 10 mL vial equipped with a stir bar. [Cu^{I}(CH_3CN)$_4$](PF_6) (54 mg, 0.14 mmol) was added to the ligand solution. After 30 min, Et_2O (20 mL) was added to precipitate the complex as a white powder (60 mg, 70% yield). ^{1}H NMR (acetone-d_6): 8.59 (m, 1H, Py−H), 8.01 (m, 1H, Py−H), 7.59 (m, 1H, Py−H), 7.52 (m, 1H, Py−H), 4.88 (m, 2H, NCH_2Py), 3.48 (m, 2H, C−H), 2.82 (m, 2H, C−H), 2.61 (m, 1H, C−H), 2.55 (bs, 1H, O−H), 2.41 (s, 3H, Cu−CH_3CN), 1.95 (m, 1H, C−H), 1.8−1.2 (m, 13H, C−H), 1.10 (m, 1H, C−H), 0.95 (m, 5H, C−H), 0.78 (s, 3H, C−H_3), 0.72 (m, 1H, C−H). Elem Anal. Calcd for $C_{27}H_{39}CuF_6N_3OP·H_2O$·acetone: C, 51.0%; H, 6.7%; N, 6.0%. Found: C, 50.5%; H, 6.3%; N, 5.7%. ESI-MS (m/z): 659.3 [M − PF_6 + $((CH_3)_2CO)_2$]$^+$.

Oxidation of Copper Complexes under Different Reaction Conditions. *Standard Procedure for Oxidation of Copper Complexes with O_2.* In the glovebox, 4 mL of an acetone solution containing 8 mg of **S1**−Cu^{I} (4 mM, 0.016 mmol) was added to a 10 mL vial equipped with a stir bar and capped with a rubber septum. Outside the glovebox, dry O_2 was bubbled through the solution for 10 s [it is noted that if the oxidation was not carried out at room temperature, the vial was placed in an oil bath (50 °C) or ice bath (0 °C) for 5 min before the injection of O_2]. After 6 h, 3 mL of an aqueous solution containing Na_4EDTA (pH = 11) was added to quench the reaction. The acetone/H_2O mixture was extracted with Et_2OAc (3 mL × 3), and the resulting organic fractions were dried with $MgSO_4$. After filtration, the organic phase was dried under vacuum. The resulting organic product was dissolved in 0.65 mL of $CDCl_3$ containing 2.3 mL of styrene (internal standard, 0.02 mmol). The reaction products were quantified by ^{1}H NMR comparing the integration of the signals corresponding to the reaction products with the integration of the signals corresponding to the internal standard. It is noted that the products derived from acetone oxidation were identified and quantified by GC analysis (see the SI for details).

Standard Procedure for Oxidation of Copper Complexes with H_2O_2. The oxidation of **S1**−Cu^{I} with H_2O_2 was carried out following a similar procedure to the one described above. Instead of bubbling O_2 through the solution, the desired amount of H_2O_2, 35%, was added using a syringe. The reaction was quenched after 30 min by adding 3 mL of an aqueous solution containing Na_4EDTA (pH = 11). Product isolation and quantification was done following the methodology described above. Similar procedures were followed for the oxidation of the different **S1**- and **S2**-derived copper complexes, with the different solvents and with the different conditions (i.e., addition of 1 equiv of Cu^{I} or NaAsc). All the results are summarized in Figures 3 and 4 and in Tables S13−S14 (SI).

Kinetic Experiments: Oxidation of Cu Complexes Following UV−Vis Spectroscopy. *Standard Procedure for Oxidation of*

DOI: 10.1021/acs.joc.7b01069
J. Org. Chem. 2017, 82, 7887−7904

Copper Complexes with O_2. A 3 mL solution of **S1**−Cu^I in acetone was placed in a 10 mm path quartz cell equipped with a stir bar, and it was capped with a rubber septum. After the cell was cooled down to 0 °C, O_2 was bubbled through the solution for 5 s. The reaction spectral changes were recorded every 2 s for 3000 s. Kinetic analysis was performed by fitting the exponential formation and decay of the different copper species at different wavelengths (see the SI for further details). A similar procedure was carried out in the oxidation of **S2**−Cu^I at −40 °C.

Standard Procedure for Oxidation of Copper Complexes with ROOH. A 3 mL solution of **S1**−Cu^I in acetone was placed in a 10 mm path quartz cell equipped with a stir bar, and it was capped with a rubber septum. After the cell was cooled down to 0 °C, 100 μL of an acetone solution containing the corresponding ROOH oxidant was added (it is noted that the solution of ROOH was deoxygenated by Ar/vacuum cycles before being injected into the Cu^I complex). Kinetic analysis was performed by fitting the exponential decay of the different LCu^{II}(OOR) species at λ = 400 nm (see the SI for further details). A similar procedure was carried out in the oxidation of **S2**−Cu^I with ROOH oxidants at −40 °C.

Kinetic Experiments: Oxidation of Cu Complexes Following the Evolution of the Reaction Yield. In the glovebox, 2 mL of an acetone solution containing the desired amounts of **S1**−Cu^I or **S2**−Cu^I was added to a 10 mL vial equipped with a stir bar and capped with a rubber septum (4 mM). Outside the glovebox, dry dioxygen (or ROOH) was added to the solution after being cooled to the desired temperature (0 °C for **S1**, −40 °C for **S2**). The reaction was quenched at the desired time by adding 3 mL of an aqueous solution containing Na_4EDTA (pH = 11). Product extraction and ^{1}H NMR analysis were carried out as previously described (see above and the SI for details).

EPR Measurements. In the glovebox, 0.5 mL of an acetone solution containing the desired amounts of **S1**−Cu^I or **S2**−Cu^I was added to a 10 mL, 7 in., 5 mm o.d. quartz tube (2 mM). Outside the glovebox, dry dioxygen (or ROOH) was added to the solution after being cooled to the desired temperature (0 °C for **S1**, −40 °C for **S2**), and the sample was subsequently frozen with liquid N_2. The spectra were recorded at 20 K. The samples were warmed up at room temperature; after 30 min, they were frozen again, and the spectra were measured, in order to evaluate the spectral changes upon decay of the LCu^{II}(OOR) species (see the SI).

Oxidation of the Copper Complexes under Different Conditions in the Presence of External Substrates (Intermolecular Oxidation Experiments). In the glovebox, 4 mL of an acetone solution containing the desired amounts of **S1**−Cu^I or **S2**−Cu^I was added to a 10 mL vial equipped with a stir bar and capped with a rubber septum (4 mM). Outside the glovebox, the external substrate (cyclohexane or 1,2-DMCH, 400 mM) and oxidant (O_2 or ROOH) were injected sequentially into the copper(I) solution. A 0.5 mL sample of the crude reaction was quenched by the addition of PPh_3 (to quench excess of ROOH);[15] internal standard was added (biphenyl, 400 mM), and the solution was analyzed by GC (see the SI for further details). A 3 mL sample of the reaction crude was quenched by adding 3 mL of an aqueous solution containing Na_4EDTA (pH = 11). Product extraction and ^{1}H NMR analysis were carried out as previously described (analysis of **S1**−OH or **S2**−OH formation, see above and the SI for details).

Analysis of the Decay Products of LCu^{II}(OOCum) Intermediates (O−O Cleavage Mechanism). In the glovebox, 4 mL of an acetone solution containing the desired amounts of **S1**−Cu^I or **S2**−Cu^I was added to a 10 mL vial equipped with a stir bar and capped with a rubber septum (4 mM). Outside the glovebox, the vial was cooled to the desired temperature (if required) and 100 μL of an acetone solution containing CumOOH (8 mM) was added (it is noted that the solution of CumOOH was deoxygenated by Ar/vacuum cycles before being injected into the Cu^I complex). After 30 min, 0.5 mL of the crude reaction was quenched by the addition of PPh_3 (to quench excess of ROOH); internal standard was added (biphenyl, 400 mM), and the solution was analyzed by GC (acetophenone and CumOH quantification, see the SI for further details). A 3 mL portion of the reaction crude was quenched by adding 3 mL of an aqueous solution containing Na_4EDTA (pH = 11). Product extraction and ^{1}H NMR analysis were carried out as previously described (analysis of **S1**−OH or **S2**−OH formation, see above and the SI for details).

Oxidation of Copper Complexes under Different Reaction Conditions in the Presence of Halogenated Solvents (Radical Trap Experiments). In the glovebox, 4 mL of an acetone solution containing the desired amounts of **S1**−Cu^I or **S2**−Cu^I was added to a 10 mL vial equipped with a stir bar and capped with a rubber septum (4 mM). Outside the glovebox, the desired halogenated solvent (CCl_4 or CCl_3Br, 400 mM) and oxidant (O_2 or ROOH) were injected sequentially into the copper(I) solution. The reaction crude was quenched by adding 3 mL of an aqueous solution containing Na_4EDTA (pH = 11). Product extraction and ^{1}H NMR analysis were carried out as previously described (analysis of **S1**−OH, **S1**−Br, and **S1**−Cl or **S2**−OH, **S2**−Br, and **S2**−Cl formation, see above and the SI for details).

Representative Procedure for Oxidation of Steroidal Picolyl Imine (S2). Copper(II) nitrate trihydrate (67 mg, 0.275 mmol, 1.1 equiv) and DHEA picolyl imine **S2** (95 mg, 0.25 mmol) were added to a reaction flask followed by THF (1.25 mL) at room temperature. The heterogeneous mixture was stirred vigorously for 30 min during which all the solids initially dissolved giving a deep blue solution, followed by the formation of a heavy pale blue precipitate. Hydrogen peroxide (0.13 mL, 1.25 mmol, 5.0 equiv, 30 wt % in H_2O) was then added to the reaction mixture dropwise which resulted in the dissolution of the precipitate to give a blue-green solution. This was accompanied by a slight exotherm and formation of gas. The reaction mixture was then stirred for 60 min at room temperature. Then, EtOAc (1.0 mL) and saturated aqueous Na_4EDTA (1.0 mL, pH ∼ 10) were added, and the reaction mixture was stirred for 15 h. The layers were separated. The aqueous layer was further extracted with EtOAc (3 × 1 mL), dried over anhydrous sodium sulfate, and concentrated *in vacuo*. The crude product was purified by flash column chromatography (SiO_2, 1:1 to 1:3 hexanes/EtOAc) to afford product **P2** as a white solid (70.6 mg, 0.232 mmol, 93%). Spectroscopic data were identical to those reported in the literature.[22]

Oxidation of Camphor Picolyl Imine (S1). Copper(II) nitrate trihydrate (58 mg, 0.24 mmol, 0.95 equiv) was added to a solution of camphor picolyl imine **S1** (61 mg, 0.25 mmol) in THF (2.5 mL) at room temperature and stirred for 15 min. The reaction mixture was then heated to 50 °C. Hydrogen peroxide (0.26 mL, 2.5 mmol, 10.0 equiv, 30 wt % in H_2O) was then added to the reaction mixture dropwise and stirred at 50 °C for 4.5 h. The reaction mixture was then cooled to room temperature; EtOAc (1.0 mL) and saturated aqueous Na_4EDTA (1.0 mL, pH ∼ 10) were added, and the reaction mixture was stirred for 15 h. The layers were separated. The aqueous layer was extracted with EtOAc (3 × 1 mL), dried over anhydrous sodium sulfate, and concentrated *in vacuo*. The crude product was purified by flash column chromatography (SiO_2, 1:1 hexanes/EtOAc) to afford the product as a white solid (48 mg, 0.185 mmol, 74%). Spectroscopic data were identical to those reported in the literature.[22]

■ ASSOCIATED CONTENT

Supporting Information

The Supporting Information is available free of charge on the ACS Publications website at DOI: 10.1021/acs.joc.7b01069.

Additional synthetic and experimental details: Figures S1−S52, Schemes S1−S24, and Tables S1−S27 (PDF)

Crystallographic data for **S1**$_2$−Cu^{II} (CIF)

Crystallographic data for **S1**−Cu^{II} (CIF)

Crystallographic data for **S2**$_2$−Cu^{II} (CIF)

Crystallographic data for **S3**−Me−Cu^I (CIF)

Crystallographic data for **S1**−Cu^I (CIF)

Crystallographic data for **S1**$_2$−Cu^I (CIF)

DOI: 10.1021/acs.joc.7b01069
J. Org. Chem. 2017, 82, 7887−7904

AUTHOR INFORMATION

Corresponding Author

*E-mail: igarciabosch@smu.edu.

ORCID

Phil S. Baran: 0000-0001-9193-9053

Isaac Garcia-Bosch: 0000-0002-6871-3029

Author Contributions

‖R.T. and Y.Y.S. contributed equally.

Notes

The authors declare no competing financial interest.

ACKNOWLEDGMENTS

I.G.-B. thanks the Robert A. Welch Foundation for financial support (grant N-1900). We thank the NIH (GM-118176 to P.S.B.), NSS (Ph.D.) A*STAR (predoctoral fellowship to Y.Y.S.), and the Hewitt Foundation (postdoctoral fellowship to A.T.H.). We thank Prof. Kenneth D. Karlin (The Johns Hopkins University) for help with the EPR and ESI-MS measurements and for insightful discussions.

REFERENCES

(1) Gutekunst, W. R.; Baran, P. S. *Chem. Soc. Rev.* **2011**, *40*, 1976.
(2) Brückl, T.; Baxter, R. D.; Ishihara, Y.; Baran, P. S. *Acc. Chem. Res.* **2012**, *45*, 826.
(3) Newhouse, T.; Baran, P. S. *Angew. Chem., Int. Ed.* **2011**, *50*, 3362.
(4) Hartwig, J. F. *J. Am. Chem. Soc.* **2016**, *138*, 2.
(5) Solomon, E. I.; Heppner, D. E.; Johnston, E. M.; Ginsbach, J. W.; Cirera, J.; Qayyum, M.; Kieber-Emmons, M. T.; Kjaergaard, C. H.; Hadt, R. G.; Tian, L. *Chem. Rev.* **2014**, *114*, 3659.
(6) Costas, M.; Mehn, M. P.; Jensen, M. P.; Que, L. *Chem. Rev.* **2004**, *104*, 939.
(7) Que, L., Jr.; Tolman, W. B. *Angew. Chem., Int. Ed.* **2002**, *41*, 1114.
(8) Oloo, W. N.; Que, L. *Acc. Chem. Res.* **2015**, *48*, 2612.
(9) Chen, M. S.; White, M. C. *Science* **2007**, *318*, 783.
(10) Cussó, O.; Garcia-Bosch, I.; Ribas, X.; Lloret-Fillol, J.; Costas, M. *J. Am. Chem. Soc.* **2013**, *135*, 14871.
(11) Conde, A.; Vilella, L.; Balcells, D.; Díaz-Requejo, M. M.; Lledós, A.; Pérez, P. J. *J. Am. Chem. Soc.* **2013**, *135*, 3887.
(12) Kirillov, A. M.; Kirillova, M. V.; Pombeiro, A. J. L. *Coord. Chem. Rev.* **2012**, *256*, 2741.
(13) (a) Huang, Z.; Lumb, J.-P. *Angew. Chem., Int. Ed.* **2016**, *55*, 11543. (b) Huang, Z.; Askari, M. S.; Esguerra, K. V. N.; Dai, T.-Y.; Kwon, O.; Ottenwaelder, X.; Lumb, J.-P. *Chemical Science* **2016**, *7*, 358. (c) Askari, M. S.; Rodriguez-Solano, L. A.; Proppe, A.; McAllister, B.; Lumb, J. P.; Ottenwaelder, X. *Dalton Trans.* **2015**, *44*, 12094.
(14) Gephart, R. T.; McMullin, C. L.; Sapiezynski, N. G.; Jang, E. S.; Aguila, M. J. B.; Cundari, T. R.; Warren, T. H. *J. Am. Chem. Soc.* **2012**, *134*, 17350.
(15) Garcia-Bosch, I.; Siegler, M. A. *Angew. Chem., Int. Ed.* **2016**, *55*, 12873.
(16) Schonecker, B.; Zheldakova, T.; Liu, Y.; Kotteritzsch, M.; Gunther, W.; Gorls, H. *Angew. Chem., Int. Ed.* **2003**, *42*, 3240.
(17) Schonecker, B.; Zheldakova, T.; Lange, C.; Gunther, W.; Gorls, H.; Bohl, M. *Chem. - Eur. J.* **2004**, *10*, 6029.
(18) Schonecker, B.; Lange, C.; Zheldakova, T.; Gunther, W.; Gorls, H.; Vaughan, G. *Tetrahedron* **2005**, *61*, 103.
(19) Fortner, K. C.; Kato, D.; Tanaka, Y.; Shair, M. D. *J. Am. Chem. Soc.* **2010**, *132*, 275.
(20) Giannis, A.; Heretsch, P.; Sarli, V.; Stößel, A. *Angew. Chem., Int. Ed.* **2009**, *48*, 7911.
(21) Rabe, S.; Moschner, J.; Bantzi, M.; Heretsch, P.; Giannis, A. *Beilstein J. Org. Chem.* **2014**, *10*, 1564.
(22) See, Y. Y.; Herrmann, A. T.; Aihara, Y.; Baran, P. S. *J. Am. Chem. Soc.* **2015**, *137*, 13776.
(23) Liu, J. J.; Diaz, D. E.; Quist, D. A.; Karlin, K. D. *Isr. J. Chem.* **2016**, *56*, 738.
(24) Rolff, M.; Schottenheim, J.; Peters, G.; Tuczek, F. *Angew. Chem., Int. Ed.* **2010**, *49*, 6438.
(25) Becker, J.; Gupta, P.; Angersbach, F.; Tuczek, F.; Näther, C.; Holthausen, M. C.; Schindler, S. *Chem. - Eur. J.* **2015**, *21*, 11735.
(26) Lewis, E. A.; Tolman, W. B. *Chem. Rev.* **2004**, *104*, 1047.
(27) Mirica, L. M.; Ottenwaelder, X.; Stack, T. D. P. *Chem. Rev.* **2004**, *104*, 1013.
(28) Clark, D. E. *Chem. Health Saf.* **2001**, *8*, 12.
(29) Gupta, P.; Diefenbach, M.; Holthausen, M. C.; Förster, M. *Chem. - Eur. J.* **2017**, *23*, 1427.
(30) Holland, P. L.; Rodgers, K. R.; Tolman, W. B. *Angew. Chem., Int. Ed.* **1999**, *38*, 1139.
(31) Elwell, C. E.; Gagnon, N. L.; Neisen, B. D.; Dhar, D.; Spaeth, A. D.; Yee, G. M.; Tolman, W. B. *Chem. Rev.* **2017**, *117*, 2059.
(32) Itoh, S. In *Copper-Oxygen Chemistry*; Itoh, S., Karlin, K. D., Eds.; John Wiley & Sons, Inc.: Hoboken, 2011; p 225.
(33) Beeson, W. T.; Phillips, C. M.; Cate, J. H. D.; Marletta, M. A. *J. Am. Chem. Soc.* **2012**, *134*, 890.
(34) Peterson, R. L.; Himes, R. A.; Kotani, H.; Suenobu, T.; Tian, L.; Siegler, M. A.; Solomon, E. I.; Fukuzumi, S.; Karlin, K. D. *J. Am. Chem. Soc.* **2011**, *133*, 1702.
(35) Lee, J. Y.; Peterson, R. L.; Ohkubo, K.; Garcia-Bosch, I.; Himes, R. A.; Woertink, J.; Moore, C. D.; Solomon, E. I.; Fukuzumi, S.; Karlin, K. D. *J. Am. Chem. Soc.* **2014**, *136*, 9925.
(36) Kunishita, A.; Kubo, M.; Sugimoto, H.; Ogura, T.; Sato, K.; Takui, T.; Itoh, S. *J. Am. Chem. Soc.* **2009**, *131*, 2788.
(37) Maiti, D.; Narducci Sarjeant, A. A.; Karlin, K. D. *J. Am. Chem. Soc.* **2007**, *129*, 6720.
(38) Wada, A.; Harata, M.; Hasegawa, K.; Jitsukawa, K.; Masuda, H.; Mukai, M.; Kitagawa, T.; Einaga, H. *Angew. Chem., Int. Ed.* **1998**, *37*, 798.
(39) Kunishita, A.; Ishimaru, H.; Nakashima, S.; Ogura, T.; Itoh, S. *J. Am. Chem. Soc.* **2008**, *130*, 4244.
(40) Maiti, D.; Lee, D.-H.; Gaoutchenova, K.; Würtele, C.; Holthausen, M. C.; Narducci Sarjeant, A. A.; Sundermeyer, J.; Schindler, S.; Karlin, K. D. *Angew. Chem., Int. Ed.* **2008**, *47*, 82.
(41) Hong, S.; Huber, S. M.; Gagliardi, L.; Cramer, C. C.; Tolman, W. B. *J. Am. Chem. Soc.* **2007**, *129*, 14190.
(42) Donoghue, P. J.; Tehranchi, J.; Cramer, C. J.; Sarangi, R.; Solomon, E. I.; Tolman, W. B. *J. Am. Chem. Soc.* **2011**, *133*, 17602.
(43) Hatcher, L. Q.; Karlin, K. D. *JBIC, J. Biol. Inorg. Chem.* **2004**, *9*, 669.
(44) Schaefer, T.; Schindelka, J.; Hoffmann, D.; Herrmann, H. *J. Phys. Chem. A* **2012**, *116*, 6317.
(45) Bordwell, F. G.; Harrelson, J. A., Jr. *Can. J. Chem.* **1990**, *68*, 1714.
(46) Warren, J. J.; Tronic, T. A.; Mayer, J. M. *Chem. Rev.* **2010**, *110*, 6961.
(47) Marusawa, H.; Ichikawa, K.; Narita, N.; Murakami, H.; Ito, K.; Tezuka, T. *Bioorg. Med. Chem.* **2002**, *10*, 2283.
(48) Yamada, M.; Karlin, K. D.; Fukuzumi, S. *Chemical Science* **2016**, *7*, 2856.
(49) Gary, J. B.; Citek, C.; Brown, T. A.; Zare, R. N.; Wasinger, E. C.; Stack, T. D. P. *J. Am. Chem. Soc.* **2016**, *138*, 9986.
(50) (a) The kinetic experiments cannot rule out the formation of dinuclear $L_2Cu_2O_2$ species via the initial slow formation of $LCu^{II}(O_2^{\bullet-})$ and the fast reaction with LCu^{I} (see ref 26). (b) During the kinetic analysis of the reaction between **S1**−Cu^{I} with O_2 (see SI), we noticed the presence of a second minor underlying reaction coincident with the major oxidative process.
(51) Das, D.; Lee, Y.-M.; Ohkubo, K.; Nam, W.; Karlin, K. D.; Fukuzumi, S. *J. Am. Chem. Soc.* **2013**, *135*, 2825.
(52) Fujii, T.; Yamaguchi, S.; Hirota, S.; Masuda, H. *Dalton Trans.* **2008**, 164.
(53) Fujii, T.; Yamaguchi, S.; Funahashi, Y.; Ozawa, T.; Tosha, T.; Kitagawa, T.; Masuda, H. *Chem. Commun.* **2006**, 4428.
(54) Choi, Y. J.; Cho, K.-B.; Kubo, M.; Ogura, T.; Karlin, K. D.; Cho, J.; Nam, W. *Dalton Trans.* **2011**, *40*, 2234.

DOI: 10.1021/acs.joc.7b01069
J. Org. Chem. 2017, 82, 7887−7904

(55) Fujii, T.; Naito, A.; Yamaguchi, S.; Wada, A.; Funahashi, Y.; Jitsukawa, K.; Nagatomo, S.; Kitagawa, T.; Masuda, H. *Chem. Commun.* **2003**, 2700.
(56) Kim, S.; Saracini, C.; Siegler, M. A.; Drichko, N.; Karlin, K. D. *Inorg. Chem.* **2012**, *51*, 12603.
(57) Osako, T.; Nagatomo, S.; Kitagawa, T.; Cramer, C.; Itoh, S. *JBIC, J. Biol. Inorg. Chem.* **2005**, *10*, 581.
(58) Osako, T.; Nagatomo, S.; Tachi, Y.; Kitagawa, T.; Itoh, S. *Angew. Chem., Int. Ed.* **2002**, *41*, 4325.
(59) Kitajima, N.; Katayama, T.; Fujisawa, K.; Iwata, Y.; Morooka, Y. *J. Am. Chem. Soc.* **1993**, *115*, 7872.
(60) Coggins, M. K.; Martin-Diaconescu, V.; DeBeer, S.; Kovacs, J. A. *J. Am. Chem. Soc.* **2013**, *135*, 4260.
(61) Tano, T.; Ertem, M. Z.; Yamaguchi, S.; Kunishita, A.; Sugimoto, H.; Fujieda, N.; Ogura, T.; Cramer, C. J.; Itoh, S. *Dalton Trans.* **2011**, *40*, 10326.
(62) Paria, S.; Ohta, T.; Morimoto, Y.; Ogura, T.; Sugimoto, H.; Fujieda, N.; Goto, K.; Asano, K.; Suzuki, T.; Itoh, S. *J. Am. Chem. Soc.* **2015**, *137*, 10870.
(63) (a) It is worth mentioning that the structure of the $LCu^{II}(OOR)$ intermediates described in this report is unusual but not unique. Tolman and co-workers have reported several mononuclear copper-peroxo species bearing bidentate ligands. See the following references. (b) Aboelella, N. W.; Kryatov, S. V.; Gherman, B. F.; Brennessel, W. W.; Young, V. G., Jr.; Sarangi, R.; Rybak-Akimova, E. V.; Hodgson, K. O.; Hedman, B.; Solomon, E. I.; Cramer, C. J.; Tolman, W. B. *J. Am. Chem. Soc.* **2004**, *126*, 16896. (c) Spencer, D. J. E.; Aboelella, N. W.; Reynolds, A. M.; Holland, P. L.; Tolman, W. B. *J. Am. Chem. Soc.* **2002**, *124*, 2108. (d) Reynolds, A. M.; Gherman, B. F.; Cramer, C. J.; Tolman, W. B. *Inorg. Chem.* **2005**, *44*, 6989.

DOI: 10.1021/acs.joc.7b01069
J. Org. Chem. 2017, 82, 7887−7904